COO-4051-21

MASTER

A Sourcebook on the Production of Electricity From Geothermal Energy

Draft

Chapter 4, Section 4.4

"Status of the Development of the Total Flow System for Electric Power Production from Geothermal Energy"

Material supplied by
Arthur L. (Roy) Austin
Lawrence Livermore Laboratory
Livermore, CA 94550

Material edited by
D. John Ryley
Brown University
Providence, RI 02912

April, 1978

Performed under

Department of Energy

Division of Geothermal Energy

Contract No. EY-76-S-02-4051.A001

Report No. CATMEC/15

EAB

DISCLAIMER

Editor's Note

The material for this report was supplied by Dr. A. L. (Roy) Austin for the Fifth Meeting of the Centers for the Analysis of Thermal-Mechanical Energy Conversion Concepts held at Salt Lake City, Utah, on April 12-14th 1977 and subsequently printed in the Minutes of that meeting; CATMEC/4, Appendix C.

The Total Flow Project will continue beyond that date until its termination on October 1st 1978. The report here presented is believed to reflect accurately the status of the Project as at the end of the year 1977.

The contents of the present report follow closely the statements in CATMEC/4, Appendix C, the Nomenclature and Glossary being supplied by the Editor who also made minor amendments to the text to secure clarity and continuity.

I am indebted to Dr. Austin for supplying prints and answering patiently many queries.

D. J. Ryley

March 30, 1978

Division of Engineering

Brown University

Providence, RI

NOMENCLATURE

B	Blade width	m
C	Coefficient	
D	Wheel diameter	m
F	Aerodynamic drag	N
P	Absolute pressure	MPa
T	Absolute temperature,	K
	Thrust	N
U	Velocity	m/s
V	Velocity	m/s
a	Liquid fraction removed radially	
d	Droplet diameter	m
e	Efficiency, loss	
f	Moody friction factor	
g	Gravitational constant	m/s^2
l	Specific enthalpy	kJ/kg
s	Specific entropy	kJ/kg K
t	Temperature,	°C
	Time	s
u,v	Velocities	m/s
x	Dryness fraction	

α	Angle defined on Fig. 4-10	
β	Blade speed/Nozzle steam speed	
η	Nozzle velocity coefficient	
λ	Velocity ratio	
μ	Viscosity	kg/m s
ρ	Density	kg/m^3
$\dot{m}$	Flowrate	kg/s
$\dot{Q}$	Enthalpy rate	kJ/s
r,θ	Polar coordinates	
C_D	Drag coefficient	

Subscripts, etc.

b	Blade
c	Loss arising from radial removal of liquid
d	Loss arising from disk friction
e	Engine, exhaust
l	Liquid
r	Relative
s	Isentropic
t	Turbine
T	Thrust
v	Vapor
w	Turbine wheel
o	Reservoir
1,2,3...	State points
Δ	Finite change in...

A prime (') denotes a polytropic

A bar ($\bar{}$) denotes a vector quantity

CONTENTS OF SECTION 4.4

4.4.1. Introduction

Events during the last few years have focussed worldwide attention on the increasing need for clean, inexpensive energy supplies with particular emphasis on development of non-fossil sources. In the U.S.A., geothermal energy is currently receiving wide interest as one such alternate energy source, particularly for electric power generation. Geothermal energy is defined here as the thermal energy stored in deposits of dry steam, hot water, and hot dry rock. Although dry steam deposits are technologically the easiest to exploit, their occurrence is estimated to be only about one-twentieth as common as hot water deposits. On the other hand, while there may be immense amounts of energy stored in hot dry rock, no technology yet exists for recovery of this energy nor has significant exploration been carried out yet to determine if and where exploitable deposits exist. Consequently, during the next decade geothermal energy development in the U.S. will likely emphasize exploitation of the water-dominated resource.

Temperatures of the water deposits of primary interest vary from 150°C to 300°C with total dissolved solids (TDS) ranging from less than 0.1% to over 25%. Although these resources constitute a significant energy resource, there are two major constraints that will influence the rate of development. First, the range of chemical conditions encountered will likely require special conversion systems. In some cases, economic utilization of high temperature-high salinity brines has not yet been proven feasible. Second, economic considerations require development of conversion machines with highest efficiencies in order to minimize the number of wells per unit of electrical capacity. In the U.S. an accelerated effort is currently underway, supporting a broad-based research and development program. Much of this work is directed toward new conversion systems in an attempt to increase opportunities for utilization of hostile fluids and for improved economics.

4.4.2. Characteristics of Wellhead Fluids

Before proceeding, it is of value to summarize briefly the nature of the fluids produced by hydrothermal wells. During the last ten years, considerable attention has been given to understanding hydrothermal systems and the characteristics of well flow from hot water deposits. Models of hot water systems have been described by Muffler and White (1972), White (1973), Facca (1973), James (1967, 1970, 1970), and Gould (1974), among others, in which mechanisms are proposed for production from hydrothermal systems which are hot enough to produce two-phase flow by flashing in the wellbore.

Since limited data are readily available to illustrate a wide variety of conditions, an approximate evaluation is relatively easy to obtain by numerical solution of the momentum and continuity equations for adiabatic steady flow up a well. Table 4-1 lists the results of such calculations [Austin et al., 1973 and Johnson, 1974]. The reservoir conditions and assumed conditions for well design were chosen arbitrarily, but are generally representative of field conditions. The well flow rates calculated are those at the well head pressures for which the thermal energy extraction rate is maximum. Actual fluid production rates and energy content, however, will be adversely affected by the presence of dissolved solids. It is estimated [Grens, 1975] that for each 1.0% increase in these dissolved solids, there may be a reduction of up to 0.8 to 0.9% in energy extraction rate, but experimental verification of these calculations is needed. Nevertheless, neglecting this condition the characteristics given in Table 4-1 are found to be reasonably consistent with the limited data available in the literature and will be used here as the basis for any system calculations appearing in this chapter.

There are two reasons to consider downhole pumping. One is to increase production from low temperature deposits, and the other is to maintain liquid

TABLE 4-1

Calculated Geothermal Well Characteristics for the Self-Pumping Mode of Production

Reservoir Temperature		Wellhead Characteristics						
		Temperature		Pressure		Vapor	Enthalpy	
°C	(°F)	°C	°F	MPa	($\frac{lb}{in^2}$)	Fraction %	$\frac{kJ}{kg}$	($\frac{Btu}{lb}$)
177	(351)	138	(280)	0.344	(50)	7.4	740.1	(318.2)
204	(399)	163	(325)	0.676	(98)	8.3	862.9	(371.0)
260	(500)	199	(390)	1.517	(220)	13.7	1113.4	(478.7)
300	(572)	223	(433)	2.482	(360)	18.9	1308.4	(562.5)

Reservoir Temperature		Flow rate in (See footnote 2)				Thermal Energy Extraction Rate (See footnote 3)			
		f = .02		f = .04		f = .02		f = .04	
°C	(°F)	$\frac{kg}{m^2 s}$	$\frac{lb}{ft^2 s}$	$\frac{kg}{m^2 s}$	$\frac{lb}{ft^2 s}$	$\frac{MW_t}{m^2}$	$\frac{MW_t}{ft^2}$	$\frac{MW_t}{m^2}$	$\frac{MW_t}{ft^2}$
177	(351)	1708.9	(350)	1391.5	(285)	914.9	(85)	742.7	(69)
204	(399)	2270.4	(465)	1830.9	(375)	1496.2	(139)	1205.6	(112)
260	(500)	2978.3	(610)	2319.2	(475)	2701.8	(251)	2109.7	(196)
300	(572)	3222.5	(660)	2441.3	(500)	3552.1	(330)	2691.0	(250)

NOTES: 1. Well depth 1524 m (5000 ft.), Production casing 0.194 m (7 5/8 in) O.D., 0.172 m (6.77 in) I.D., Area = 0.023 m^2 (0.25 ft^2).

2. Calculations are based on thermodynamic properties of pure water, f = Moody friction factor.

3. The thermal energy extraction rate is calculated with reference to saturated liquid enthalpy at 48.9°C (120°F), In S.I. Units, $\dot{Q} = \dot{m}\ (h_2 - 205)$, fps Units, $\dot{Q} = \dot{m}\ (h_2 - 87.9)$

4. Condensing temperature 49°C.

5. The gross power output is debited 10% to provide power for internal plant pumping.

flow from higher temperature deposits. This may be especially important to suppress precipitation and scale formation in surface equipment associated with the Binary Cycle concept [Chapter 4]. For the application in the higher temperature brines, problems of reliability are particularly serious. As yet, proven pumps have not been demonstrated. There are several concepts under development, and this work should be encouraged.

4.4.3. Energy Conversion Concepts

For recovery and conversion of the energy in water-dominated resources, only three basic conversion concepts exist. These are: (a) the flashed steam system, (b) the binary cycle concept, and (c) the total flow concept. A fourth concept envisages combinations of these systems, i.e. hybrid systems [ ]. For electric power generation, the development of hybrid systems may be necessary to achieve the most effective utilization of hydrothermal resources. This may be especially the case, for example, where large amounts of non-condensible gases exist, or where unique conditions are present allowing both electrical and non-electrical uses of the energy. Any serious consideration of hybrids, as defined here, however, must begin with a thorough understanding of individual system components over the complete range of operating conditions. Hence, the development of hybrids awaits further development of the basic concept.

Currently, only the flashed steam system is in commercial use. The binary cycle concept has not yet found application, nor has even a small complete system been field-tested in the United States. The total flow concept has been the subject of considerable laboratory tests, but also has not yet been field-tested. Consequently, only the flashed steam system will be used here for performance comparisons. For that reason, a short discussion of the basic features of the flashed steam system is now presented as preparation

for the following detailed discussion of the total flow concept. Further information on flashed steam systems is given in this Chapter, Section 4.

4.4.3.1. The Flashed Steam System

In the early 1960's, New Zealand pioneered the large-scale recovery and conversion of energy in hot water deposits using the Flashed Steam method [Chapter 12]. A great deal of information has been published, and operational flashed steam power plants now exist in several other countries [Chapter 12]. Consequently, the technology can be considered proven, and future advances will likely lie in areas of more refined system components, power system economics, and reservoir management techniques. Since this is the only proven system with a substantial operational history, its general performance characteristics will be used here as a basis for comparison of future concepts.

Figure 4-1A illustrates schematically the elements of single flash system. Isenthalpic pressure reduction of the wellbottom product occurs prior to and at entry to the flash separator which separates the vapor and liquid fractions. The accompanying Temperature-Entropy chart in Fig. 4-1B illustrates the basic thermodynamic process involved. For simplicity, the pressure drop between separator and turbine inlet is neglected here since it is largely dependent on well spacing and detailed plant design. The most obvious point is that a substantial fraction of the available energy is discarded in the separated liquid.

Overall plant thermal efficiencies are generally below 10% for a single flash system. Greater utilization of the fluid energy, however, can be achieved with multiple flashing. [This Chapter, Section 4.1.]

For high salinity brines, carryover of solids into the vapor fraction is considered a serious limitation to the Flashed Steam system. Consequently, associated technical advances are needed in the areas of improved methods of

separation or scrubbers to minimize carryover of solids in the steam fraction, and ways to increase tolerance of conventional steam turbines to entrained solids.

In order to allow comparison of the various concepts in a later section, the performance of the Flashed Steam system is now estimated for the wellhead fluids in Table 4-1. A condensing temperature of 29°C and a 10% reduction in power output to account for internal plant pumping requirements is assumed. Results are shown in Fig. 4-2 in terms of the resource utilization, kWh/metric ton of wellhead output, i.e., the net specific energy output.

4.4.3.2. The Total Flow Concept

Based on fundamental thermodynamic principles, a direct expansion from wellhead to sink condition has the potential for conversion of the greatest fraction of the available energy. Comparison of Fig. 4-3 with Figure 4-1B indicates that the Total Flow process (expansion from 2 to 3) provides an upper bound on system efficiency. For example, regardless of the number of stages of separations used in the Flash Steam System, there will always be some useful energy discarded with the separated liquid in the last flash stage. Although the Total Flow concept is simple, and would provide the most direct means of geothermal energy conversion, it will require the development of efficient, reliable machines for two-phase expansion of the wellhead fluid.

The concept is not new, but until now practical applications have been lacking. It is believed that the first published documentation on tests of a Total Flow device consist of some brief comments by Naymanov (1970). In his paper on the flashed steam plant at Pauzhetka, he makes reference to limited tests on a hydraulic turbine operated directly from the wellhead products. He also notes that the machine tested was far from optimum and that improvements are expected. The potential performance of a Total Flow process is shown in Fig. 4.2.

It should be emphasized here that this comparison is based only on thermodynamic considerations, and the assumptions used for the respective engine efficiencies of the systems shown. Figure 4.2 shows that to gain the advantages shown, a total flow expander must have an engine efficiency of 70%, a performance as yet unrealized, but the performance of steam turbines for geothermal applications may increase as geothermal energy developments proliferate. Not withstanding the poor performance to date, the potential for the Total Flow concept appears especially promising because of its simplicity, and hence potentially lower capital costs. It should also be noted that Figure 4-2 illustrates comparison of processes, not machines. It is not yet known if the same total flow expander would work at 70% efficiency over the working fluid temperature/enthalpy range shown. It may be that different expanders will be needed at the lower temperature range than that at the higher range. More research and testing of candidate expanders over all working fluid conditions needs to be completed before this basic question can be answered. Because of the potential importance of the total flow process and because its development will add a third dimension to geothermal conversion technology, the balance of this chapter will concentrate on the required features of total flow expanders.

Total Flow Expander Characteristics

The geothermal environment demands design simplicity and flexibility to allow use of corrosion/erosion resistant materials, incorporation of precipitation and scale control methods [Chapter 6 and 7], and a means to minimize capital costs [Chapter 11]. Also, in order to gain the full advantages of the Total Flow process, it is necessary to extract the maximum available energy from the wellhead product by expansion to as low a backpressure as possible. It can be shown that for each wellhead condition listed in

Table 4-1, 40% of the useful work is obtained by expansion below atmospheric pressure to the sink condition of 49°C (3.5" Hg). Volume expansion ratios of the fluid range from about 300 (for 300°C fluids) to about 70 (for the 177°C fluids). This compares with expansion ratios of 50 to 20 for flashed steam turbines operating from the vapor fractions of the same wellhead fluids. Consequently, the Total Flow expander must be capable of complete expansion to recover the available energy, and must also be able to accommodate large volume flow rates. In addition to these requirements, candidate expanders must be able to withstand the presence of significant quantities of dissolved solids. Precipitation of silica and heavy metal sulfides during expansion can cause rapid formation of scale, and the corrosive and erosive actions of the brines will be major problems. These will likely require design simplicity, particularly with respect to minimizing the number of moving parts and swept surfaces, ease of maintenance, and long-term reliability. A single stage expander is most desirable, but staging may be feasible in some cases.

Table 4-2 lists the basic classes of expanders which have been considered for use in the Total Flow process. It is not possible here to give a detailed description of each, nor is this the only way to classify them. However, two types should be first treated individually: pure reaction machines and the multiple-disk (or bladeless) turbine.

Impulse/Reaction Machines

Generally, reaction devices are expected to find limited application. Since a pressure and temperature drop is required in the rotating component, scale formation, if it occurs, will be difficult to control or remove. Further, maximum power output requires a high ratio (approaching unity) of tip speed to absolute fluid nozzle exit velocity which leads to high speeds and high stresses. In addition, there are practical problems of maintaining rotation seals, of

modifying the geometry as wellhead pressure drops with time, and of lowered nozzle efficiency due to segregation of liquid and vapor in the rotating passage. For saturated liquid inlet conditions, however, enthalpy drop is lower across the turbine; hence, rotational speed is lower, resulting in reduced working stresses. Depending on the achievable nozzle efficiency under these conditions, the radial outflow turbine (Hero's turbine) may be a practical candidate expander.

The multiple-disk turbine consists of a series of closely spaced thin disks mounted side by side on a shaft. Fluid enters through nozzles and is injected into the spaces between the disks to follow an inward spiral path to a central exhaust port. During this passage, the fluid exerts a frictional shear stress on the disks, resulting in a net torque on the shaft. Since no detailed analysis for two-phase flow operation has been made, it is not possible to comment on the applicability of this device. Since the basic mechanism for transfer of momentum is frictional drag, and the possibility that the entrained liquid droplets will be thrown radially outward by centrifugal forces, one can only speculate that turbine efficiencies may be low. Considerable work has been done to analyze similar machines for operation from singl-phase fluids. The reader is referred to Rice (1975) for these details, and to Possell (1973) for information on machines he has built.

Positive-Displacement Machines

As a class, positive-displacement expanders are limited in volume flow-rate capacity relative to turbo-machines. Fundamentally this is due to internal losses related to sonic velocity in the fluid. Consequently, these expanders must be physically large to produce significant power output.

The helical rotor expander is a positive-displacement device which operates by direct expansion of the two-phase fluid through meshing rotors, as

TABLE 4-2

Classes of Expanders for Total Flow Applications

1. Impulse/reaction machines

   Axial flow - Curtis/Rateau steam turbine
   Radial inflow - Francis turbine and multiple disc drag turbine
   Radial outflow - rotating nozzle (pure reaction). Hero's turbine multiple disc turbine - bladeless impulse or reaction drag turbine.

2. Positive displacement machines

   Helical screw expander
   Rotating oscillating vane machine

3. Impulse machines

   Tangential flow - Pelton wheel, Re-entry turbine
   Axial flow - DeLaval, Curtis turbine

shown in Fig. 4-4. The fluid enters through a nozzle control valve into the high pressure pocket at A. As the rotors revolve, the pocket elongates continually, giving rise to a successively increasing volume from B to E, where exhaust occurs. This device is mechanically simple, and has the advantage of self-cleaning as a result of rotor-to-rotor and rotor-to-case relative motion. McKay and Sprankle (1974) have reported operating experience with a helical rotor machine expanding brines in the Cerro Prieto and East Mesa geothermal fields. They reported that no scale deposition problem had been detected during over 1000 hours of operation. This unit also has recently undergone a series of clean-water tests at the Lawrence Livermore Laboratory Geothermal Test Facility in order to investigate the mechanical performance under a range of inlet fluid thermodynamic conditions [Weiss, et al., 1975].

The unit tested was an air compressor unit with 152.4 mm (6-inch) rotors modified by R. Sprankle of the Hydrothermal Power Co., Ltd. Inlet pressures to the rotors was varied from 168 kPa (24.4 psia) to 527 kPa (76.5 psia), with vapor fractions (quality) ranging from 11.6% to 33.3%. In all tests the exhaust pressure was one atmosphere. Maximum engine efficiencies of 49% at 16 kW for 3000 rpm, 53% at 23 kW for 4,000 rpm, and 55% at 30 kW for 5000 rpm were observed. The latter figure corresponded to a utilization rate of 104 kg/kWh (228 lb/kWh).

It was concluded that the helical rotor expander is a viable candidate machine for conversion of energy from hydrothermal wells by the Total Flow process. Additional experimental work is in progress at the Lawrence Livermore Laboratory to explore the complete operating characteristics of another machine designed specifically for the geothermal hybrid applications.

In addition, House (1976) has completed an analysis of potential applications for the helical rotor expander. He concludes that engine efficiencies will generally be below 70% because of an expansion ratio limitation of 15 and

a maximum pressure differential of 758 kPa (110 psi) imposed by conductions of mechanical strength. With reference to the reservoir conditions in Table 4-1, he calculates expander sizes for single stage expansion to 49°C. His results indicate that a 40 MWe machine will have rotor diameters varying from 12.7 m (41.6 ft) to 9.0 m (29.6 ft) with lengths varying from 19.0 m (62.4 ft) to 13.5 m (44.4 ft), respectively. For a 10 MWe output, these sizes are reduced by half. These larger sizes can be reduced to more reasonable values by staging or by using the expander in combination with vapor turbines. It appears that, because of the large sizes required for single stage expansion to sub-atmospheric conditions, more suitable applications for the helical rotor expander are for non-condensing, low-power output uses or in hybrid systems with helical rotor exhaust pressures above one atmosphere (See also Elliott, 1975).

Further work is required and is in progress to more completely investigate the potential of these mechines for specific applications. The high capital loss resulting from the unavoidably large physical dimensions of positive displacement devices may limit their use for central power generation.

Impulse Machines

Based on the present understanding of all requirements, and particularly the need for inherently simple, compact machines, pure impulse devices have significant advantages. Because of geometric considerations the axial flow machine currently appears to be the most promising configuration for the Total Flow application. Figure 4.5 is a simplified view of an axial flow impulse turbine, and also illustrates the basic elements of other impulse machines. Expansion of the two-phase wellhead product through a converging-diverging nozzle converts the brine thermal energy at high wellhead pressures at 2 to kinetic energy in the form of a high velocity fluid stream at the backpressure 3'.

The nozzle velocity coefficient, η, is the ratio of actual velocity to the ideal exit velocity from an isentropic expansion from 2-3, both velocities being taken for a homogeneous mixture. The wheel efficiency, e_w, is a measure of the ability of the wheel to convert the fluid kinetic energy to shaft work. It is a complex function of blading geometry, turbulence, fluid friction, entrance and exit losses, fanning losses, etc. The turbine engine efficiency, e_t, then will be $\eta^2 e_w$, as noted in Fig. 4.5. The factor η^2 represents the nozzle efficiency, or its ability to convert thermal energy into kinetic energy.

It is clear that the basic problem of designing an efficient total flow impulse turbine is twofold: development of efficient nozzles for expansion of two-phase fluids, and development of efficient blading for momentum transfer.

Nozzle Development

For years the conventional wisdom has been that the presence of more than about 5% moisture in steam will severely reduce expansion efficiency due to slip between phases. This view has been widely held and probably has been the result of the historical technical direction taken in the steam turbine industry. It is instructive to think in terms of the right- and left-hand side of the T-s diagram for steam. Typically, conventional steam power systems involve expansion of saturated or superheated steam where the process traverses lines of decreasing quality during the expansion to subatmospheric pressures; i.e., liquid droplets are created by condensation during the expansion. For geothermal applications, the expansion (see Fig. 4-3) takes place on the left side of the T-s chart, where lines of increasing quality are traversed; i.e., liquid is being eliminated by evaporation during the expansion. Consequently, in the latter case, the liquid fraction is diminishing and the liquid masses whether entrained or swept along flow boundaries tend to decrease in size and segregate.

For example, for 18% quality inlet to 34% quality exit, the liquid droplets would, if dispersed and monodispersed in size, occupy only about 0.02% of the volume and would be spaced, on the average, tens of droplet diameters apart. This is contrary to conventional steam power experience of the right-hand side expansion where liquid is created, and droplets tend to agglomerate. Consequently, it appears that the conventional wisdom may not apply to expansion of low-quality steam, and that nozzles can be designed with high velocity coefficients for this process.

As part of the experimental work at the Geothermal Test Facility [Weiss and Shaw, 1975] at Livermore Alger,[1975], in order to develop high efficiency nozzles, has recently designed and tested nozzles of circular cross-section, and has measured nozzle thrust coefficients in the 0.92 to 0.95 range. This has increased confidence that development of turbine nozzles with coefficients greater than 0.9 can be achieved.

Experimental thrust coefficients C_T are presented in Figs. 4-6 and 4-7 as a function of nozzle backpressure. The different curves demonstrate the effects of various nozzle inlet pressures and qualities while the inlet enthalpy remained substantially constant (Maximum variation = ± 23 kJ/kg). The graphs include data for nozzles #2, #3, and #4.(Fig. 4-8), since the experimental errors involved made it impossible to distinguish differences between the respective data for each nozzle, as initially expected.

By comparing Fig. 4-6 and 4-7 it is seen that the nozzles appear to operate more efficiently at higher plenum chamber pressures for a given back pressure. Probably the factors with the greatest influence on this phenomenon are the complex shock wave processes occurring for the different operating conditions. However, all the curves approach the optimum operating conditions with thrust coefficients in the 92-94 percent range. As previously indicated, this represents nozzle efficiencies in the range of 85-88%. The silhouette of

the issuing jet was photographed under conditions of varying back pressure ranging from over-expansion through design to under-expansion. It was confirmed that the peak thrust location corresponds to the operating condition where no shock or expansion waves are present.

Additional analytical work on two-phase nozzle design [Comfort, et al., 1976] and fundamental mechanics of two-phase flow, further verify the conclusion that two-phase expansion can be efficiently accomplished by correct nozzle design. Experimental work is also continuing on development and testing of nozzles with square cross-section for application to the geometric requirements of the impulse turbine schematically illustrated in Fig. 4-5. Preliminary test results of square cross-section nozzles indicate that this geometry causes no significant loss in performance [Alger, 1976].

It should be noted, however, that most of the work to date has centered around design of machines uniquely suited for the thermodynamic conditions of the high temperature resources in the Imperial Valley; i.e., the 300°C reservoirs with wellhead conditions listed in Table 4-1. Work is in progress to explore application and design of total flow expanders and systems for the lower temperature fluids, but finalized results are not yet available.

Momentum Transfer in the Turbine Blading

One of the main factors contributing to losses in wheel efficiency is the interaction of liquid droplets with the turbine blade during passage of the two-phase supersonic flow. As a result of experimental work and analytical studies, [Comfort, 1977] has estimated the range of possible wheel efficiencies, as shown in Figure 4-9. The lower bound represents very conservative conditions as noted, while the upper bound represents an ideal efficiency based on geometry alone. There is some preliminary experimental evidence that droplet sizes less than 6 microns may be typical. The point of

Figure 4-9 is that there is a wide latitude of possibilities, and much experimental work is yet to be done before wheel efficiencies can be more accurately determined. It should be noted in passing, however, that even if the lower bound of 55% cannot be exceeded, the Total Flow process via the impulse turbine competes favorably with the single flash system. This may have future significance since the Total Flow concept may be the only possibility for utilization of the high temperature, but high salinity, brines.

The fundamental problem is to produce for inlet to the blade entrained liquid subdivided into droplets small enough to allow the vapor drag forces to direct them around the blade curvature without deposition. If liquid strikes the blade it adheres and is thrown radially outward (Coriolis loss) causing a loss in efficiency. Assume that the liquid content enters the blade as a size-monodisperse population of droplets of diameter d. If drop collision, coalescence and deposition is absent, it is a straightforward task to write the equations of motion for droplet traversal as shown below.

Referring to Fig. 4-10,

$$F_{drag} = \frac{1}{2} \rho_v C_P \left(\frac{\pi d}{4}\right)^2 (\bar{U}_V - \bar{U}_d) \, |\bar{U}_v - \bar{U}_d|$$

$$V_{rel} = \sqrt{\left(U_{V_\theta} - U_{d_\theta}\right)^2 + \left(U_{V_r} - U_{d_r}\right)^2}$$

$$= \sqrt{\left(U_{V_\theta} - r \frac{d\theta}{dt}\right)^2 + \left(U_{V_r} - \frac{dr}{dt}\right)^2}$$

$$C_D = f \left(\frac{\rho_v V_{rel} d}{\mu_v}\right)$$

$$F_{drag\ \theta} = |\bar{F}_{drag}| \cos \alpha \ , \quad F_{drag\ r} = |\bar{F}_{drag}| \sin \alpha$$

$$\cos \alpha = \frac{U_{v\theta} - r\, d\theta/dt}{V_{rel}} \quad ; \quad \sin \alpha = \frac{U_{vr} - \frac{dr}{dt}}{V_{rel}}$$

The equations of motion are:

$$\theta : \frac{1}{2}\left(\frac{\pi d^2}{4}\right)\rho_v C_D\left(U_{v\theta} - \frac{r d\theta}{dt}\right) V_{rel} = \rho_d\left(\frac{\pi d^3}{6}\right)\left(r\frac{d^2\theta}{dt^2} + 2\frac{d\theta}{dt}\frac{dr}{dt}\right) \qquad (4\text{-}1)$$

$$r : \frac{1}{2}\left(\frac{\pi d^2}{4}\right)\rho_v C_D\left(U_{vr} - \frac{dr}{dt}\right) V_{rel} = \rho_d\left(\frac{\pi d^3}{6}\right)\left(\frac{d^2 r}{dt^2} - r\left(\frac{d\theta}{dt}\right)^2\right) \qquad (4\text{-}2)$$

Numerical solution of these two coupled equations give droplet trajectories for a given droplet size, initial slip, vapor velocity, and blade curvature. Experimental work has been completed on characterizing droplet/blade interactions, and effects on blade efficiency; i.e., the ability of the blade to transfer the momentum of the two-phase flow from the nozzle. Currently, this consists primarily of static blade testing with the apparatus, shown in Fig. 4-11, which allows both blade thrust and pressure distribution measurements. The nozzle is designed to produce a fluid velocity equal to the relative fluid velocity over a moving blade so that the static test system is an approximate kinematic equivalent of the actual conditions. This device will be used for detailed investigations of droplet/blade interactions, blade configurations, and verification of analytical techniques to be ultimately used for turbine design.

The results of these experiments indicate that the droplet trajectory profiles generally follow the calculated paths by comparing photographs of the flow around blades (statically positioned) with the calculated trajectories as shown in Fig. 4-12. These experiments and additional analytical work on droplet/blade interaction and two dimensional/two-phase flow indicate that droplet sizes, for the test conditions relevant to the 300°C fluids (Table 4-1), are between 2 and 10 microns, with the average being about 6 microns.

The major research effort will be directed towards reducing droplet diameters to less than 1 micron. The effect of droplet size on wheel efficiency is shown in Fig. 4-13. The lower dashed curve is consistent with Fig. 4-10 for a symmetric blade of 0.1016 m (4") axial width, B_o. The significant point here is that even if droplets cannot be reduced to less than a micron, increasing blade width will partially compensate by adding about 10% to the wheel efficiency. The major gain in efficiency, of course, will be made by droplet size reduction. There are several methods for droplet breakup currently being investigated. Final conclusions on achievable engine efficiencies must await the results of this work and testing of turbines of advanced design, incorporating the necessary features for droplet breakup. In order to determine the applicability of the impulse turbine for two-phase flow, performance tests of a specifically designed turbine have been completed.

Performance Tests

A single stage, axial flow, impulse turbine has been designed and tested at reduced output, since only a single nozzle was used - about 5% admission (Comfort, 1977). A special rotor was built so that wide blades with sharp leading and trailing edges could be designed in anticipation of special problems associated with two-phase fluid dynamics. Blade width was made large to increase the radius of curvature of the flow path so that droplets would have a maximum probability of passing between the blades without impacting their surfaces. Sharp edges were necessary in order to minimize phenomena associated with supersonic relative velocities within the blade passage.

TABLE 4-3

Test Conditions

Fluid state at nozzle entrance

P_o = 2.53 MPa (367 lb/in^2)

x_o = quality = 14%

T_o = 224°C (434°F)

h_o = 1.2 MJ/kg (526 Btu/lbm)

$\dot{m}$ = 0.59 kg/s (1.31 lbm/s)

Exhaust pressure and temperature

P_e = 0.0137 MPa (2 lb/in^2)

T_e = 126°F

In order to simplify construction, shorten development time, and to minimize costs, the rotor was designed with integral blades and was fabricated from a 7075-T6 aluminum forging. Aluminum was chosen for its high strength-to-weight ratio and machinability.

Fig. 4-14 shows the rotor before an electroless nickel plating was applied to the blade surfaces for water droplet erosion protection. The plated rotor is not suitable for brine exposure. It was designed only to have sufficient life for the laboratory testing program. The final machining on the rotor hub was completed after plating and the finished part was then assembled with the steel shafting. The rotor assembly was balanced, and assembled into the rotor housing (Fig. 4-15). A single nozzle was used for the machine because of limited flow-rate capabilities of the test facility. The nozzle was suspended with a four-bar linkage so that axial thrust could be measured independently during performance testing of the expander, Fig. 4-16.

A dynamometer assembly, consisting of a hydraulic pump/motor was used both as a brake and as a motive source. Performance of the expander was measured by using the brake mode, while disk friction and windage losses were measured by using the hydraulic motor to drive the rotor.

The operating conditions used for the performance testing are summarized in Table 4-3. These operating conditions are selected to be representative of the thermodynamic conditions of well outputs from the reservoirs of the Salton Sea Geothermal Field.

The maximum engine efficiency for the single-nozzle test was observed to be 23% at a blade speed ratio (the ratio of the mean blade speed to the homogeneous isentropic mixture velocity of the fluid exiting the nozzle) of 0.24. Testing was done on three separate occasions and showed good

repeatability. Operation was smooth and quiet. The nozzle thrust coefficient was 0.83 during testing with the rotor. This was lower than the 0.94 thrust coefficient measured during previous tests of the nozzle alone. The nozzle thrust coefficient, C_T, is defined as:

$$C_T = \frac{T}{\dot{m}V_s} \tag{4-3}$$

where T is the measured thrust, $\dot{m}$ is the measured mass flow rate, and V_s is the homogeneous mixture isentropic velocity. Although radial pressure gradients associated with blade rotation are not as severe in two-phase conditions as would be expected in standard vapor turbines, they were probably large enough to explain the lower performance. Larger separation between the nozzle and rotor as well as improved nozzle design should eliminate this problem.

A numerical model was developed and was used to predict expander performance. The model included calculation of droplet trajectories within the blade passage to determine what happened to the liquid. In addition to standard vapor turbine losses, special losses associated with droplet impact and removal from the blades were included in the model. Static cascade measurements in two-phase flow were used to determine the performance of blades identical to those on the rotor. This information was used to normalize the vapor flow portion of the model. Measured values of combined disk friction and windage were used to normalize the disk friction and windage model in the predictive technique.

The model was designed to allow extrapolations of performance both for full admission and for changes in droplet diameter. Single-nozzle performance predictions were very successful, as will be shown, and encourage belief in the validity of the extrapolations.

The present numerical model is only adequate for impulse designs and cannot be used to select detailed blade contours because the vapor and liquids are not fully coupled; i.e., droplets are affected by the vapor, but the vapor is assumed to be unaffected by the droplets and thermodynamic effects arising from paddle work to be absent. In order to design adequately more advanced blade and nozzle contours, a completely coupled model for two-dimensions, based on an axisting one-dimensional two-phase flow calculation technique is necessary and is currently being developed.

The details (Comfort, 1977) of the numerical model are beyond the scope of this document. To provide the reader with some insight, however, into the extrapolation between the single-nozzle and full admission results, a simplified model will be presented here to demonstrate some of the characteristics to be expected.

Assuming for this simplified model that no slip exists between the vapor and liquid entering the turbine blades, one may write the expression for blade efficiency, e_b. For an impluse turbine with the ratio of mass flow rate of vapor to mixture equal to x, relative velocity coefficients for the vapor and the liquid equal to λ_V and λ_L, blade speed ratio (blade speed/ nozzle velocity) β, and nozzle angle θ to the plane of the wheel, one may write:

$$e_b = 2\beta[x(1 + \lambda_V) + (1-x)\ (1+\lambda_L)]\ (\cos\theta-\beta) \qquad (4\text{-}4)$$

where

$$\lambda_V = \left(\frac{V_{r_2}}{V_{r_1}}\right)_{\text{vapor}}, \quad \lambda_L = \left(\frac{V_{r_2}}{V_{r_1}}\right)_{\text{liquid}}$$

V_r is a relative velocity and the subscripts 1 and 2 refer to blade entry and exit.

For a given blade speed ratio and nozzle angle, no higher conversion efficiency can be achieved than that indicated by eq. (4-4) with $\lambda_V = \lambda_L = 1$. If all of the droplets impact the blade, then $\lambda_L = 0$, which reduces the efficiency of the liquid kinetic energy conversion by 50%. If some of the liquid escapes impact, the blade efficiency expression must be expanded to include those effects. To maintain a simplified approach, the analysis herein will assume that all of the liquid impacts the blade, i.e., $\lambda_L = 0$. Actual numerical results to be presented in the next section do not require this simplification.

The optimum speed ratio can be defined by differentiating e_b with respect to β and equating the derivative to zero:

$$\frac{\partial e_b}{\partial \beta} = 0 = 2[x(1+\lambda_V) + (1-x)(1+\lambda_L)][\cos\theta - 2\beta] \qquad (4\text{-}5)$$

whence

$$\beta_{optimum} = \frac{1}{2}\cos\theta$$

To convert the blade efficiency to an engine efficiency, e_t, the losses due to disk friction and to radial liquid removal, e_d and e_c, must be subtracted from the blade efficiency modified by the square of the nozzle thrust coefficient:

$$e_t = C_T^2(e_b - e_c - e_d) \qquad (4\text{-}6)$$

where

$$e_c \propto af(\beta^2)$$

$$e_d \propto g(\rho, \beta^{2.85})$$

where f, g denote "function of..."

The quantity a in the expression for the liquid removal represents the fraction of the liquid mass flow rate which must be removed radially, while ρ, in the disk friction and windage loss expression refers to the effective density of the fluid surrounding the rotor.

The ideal optimum speed ratio is valid only when the disk friction and windage, and pumping losses are small relative to the first term. For a single-nozzle test, the disk friction and windage and liquid removal losses can severely affect the blade speed ratio associated with the peak efficiency, shifting it toward a lower value. This, in turn, decreases the blade efficiency because the blade speed ratio is reduced. For full admission, the disk friction and windage loss, for a given blade speed ratio, is inversely proportional to the mass flow rate, while the liquid removal loss is proportional to the mass flow rate if all droplets impact the blade and are radially removed. Thus, the liquid removal loss is not diminished relative to power output for increased admission, whereas the disk friction and windage loss fraction is reduced. As admission is increased, the optimum blade speed ratio increases, but since the liquid removal loss is proportional to the blade speed ratio squared, the loss fraction increases.

With this brief introduction to some of the phenomena involved, the results (from the numerical model) will next be compared with the experimental results and then the numerical model will be used to extrapolate to full admission and to an advanced design. Fig. 4-17 verifies that results from the numerical model compare very well with the experimental results. As noted, the upper calculated band assumes that disk friction and windage losses are associated with the vapor density only, while the lower band assumes that they are a function of the two-phase mixture density. The upper and lower limits of each of the bands are determined by nozzle modeling uncertainty and are fully described by Comfort,[1977]. The results of static

cascade testing indicated that all entering droplets impacted the blade passages and left at negligible velocity. Droplet size estimates indicate that the droplets are probably between 2.7 and 7 microns in diameter. Results of the performance predictions indicate that they are greater than 2.2 microns because this is the largest size of droplet that can pass through the blade passage without impact. Hence, if droplets are greater than 2.2 microns in diameter, all droplets impact the blade passage -- as is indicated by the results. The blade speed ratio indicated Fig. 4-17 for the peak power point of the experimental data lies between the two calculated bands. This is significant because, as was shown, the optimum blade speed ratio for this impulse turbine is primarily dependent upon the disk friction and windage and losses associated with radial removal of liquid droplets which have impacted the blades. The fact that the optimum blade speed ratio for the bounding calculations spans the measured optimum speed ratio indicates that the mechanisms of disk friction, windage, and liquid removal are well modeled. Assuming all droplets impact the blades and are removed radially, one would expect that the vapor density would best approximate the fluid surrounding the majority of the rotor. The results indicate that this is not the case. Liquid droplets may be splashing off the rotor housing walls and remixing with the vapor, increasing the effective density of the fluid mixture around the rotor and consequently increasing the friction forces in addition to the power necessary to accelerate relatively low velocity water particles.

Fig. 4-18 shows extrapolations to a full admission performance for the existing rotor design and to an advanced design. It should be noted that the full admission results reflect the nozzle thrust coefficients previously

measured for the nozzle in the laboratory. Otherwise, the calculation contains the same parameters for the full admission calculation as for the partial admission calculation. The increase in performance is due primarily to the diminution of the effects of disk friction and windage since this loss becomes very small in comparison with full admission power input, while it is rather large compared with that of partial admission. This diminution allows the rotor to attain a higher speed ratio, enhancing the engine efficiency. Two bands are used to represent the extrapolated performance of a full admission design for droplet diameters greater than 2.2 microns, and with an assumed nozzle thrust coefficient of 0.94. The difference between the upper and lower bands (dashed and solid lines, respectively) is the result of radial liquid removal losses. The loss associated with the radial removal of liquid from the blades is included in the lower band (solid lines). Though this loss is certain in the single-nozzle design, it is not clear that it will exist in the full admission machine because the nearly continuous flow may force the liquid through the blades without significant radius change. The upper band (dashed lines) indicates the displacement of the lower band (solid lines) due to removal of the losses associated with radial pumping of the liquid from the blades. The upper bound of both bands is calculated assuming disk friction and windage loss is controlled by the vapor density and that the slip ratio (the ratio of average liquid velocity to average vapor velocity at the exit of the nozzle) is approximately 0.9. The lower bound of both bands is calculated assuming that the disk friction and windage loss is controlled by the mixture density and that the slip ratio is approximately 0.7. For the full admission performance, the slip ratio, rather than the fluid density assumed for the disk friction and windage, is the major cause of the difference between the upper and lower bounds of each band.

The advanced design assumes that the droplet size has been reduced to 1 micron, and that the thrust coefficient remains 0.94. Under these circumstances it would be expected that the liquid and vapor leave the nozzle with very nearly the same velocity. The upper bound of the lower band (solid lines) is based upon vapor turbine correlations of vapor friction losses and the assumption of vapor-controlled disk friction and windage. The lower bound of the lower band is based upon blade vapor performance consistent with results from static cascade tests and assumes that the mixture density controls disk friction and windage. The upper band for this case (dashed lines) indicates the performance if liquid radial removal losses are omitted. The change resulting from the omission is not as great as in the previous case (full admission with droplet diameters greater than 2.2 microns) because only a small fraction of the liquid impacts the blades when the droplets are 1 micron in diameter.

The single-nozzle, full admission extrapolation, and advanced design results may be compared in another way. Table 4-4 represents a summary of losses associated with the peak efficiency points corresponding to the data and extrapolations shown in Fig. 4-18. It should be remembered that this table does not indicate causality, but rather a loss summary at a particular operating condition. For example, from the single nozzle results, one might conclude that the disk friction is not a deterministic loss mechanism. However, disk friction is not an independent function, just as the other losses listed are not independent functions. In the case of disk friction, its nearly cubic relationship with blade speed ratio and its large relative magnitude compared to the power output capability of a single nozzle test forces the blade speed ratio to be considerably off-optimum. This, in turn, results in the significant loss ("geometry and non-optimum blade speed ratio") which results directly from blade efficiency relationships as previously shown.

TABLE 4-4

Loss distribution at peak efficiencies for single nozzle and for extrapolations to full admission and advanced designs.

	Single Nozzle d > 2.2 μm Percent	Full Admission* Bounds Existing Design d > 2.2 μm Percent	Full Admission* Bounds Existing Design d > 2.2 μm Percent	Full Admission* Bounds Advanced Design d ≤ 1 μm Percent	Full Admission* Bounds Advanced Design d ≤ 1 μm Percent
Loss Distribution					
Slip, Liquid/Blade, Vapor Friction	17	33	34	14	10
Liquid Pumping	2	6	0	2	0
Disk Friction and Windage	4	< 1	< 1	< 1	< 1
Geometry & Non-Optimum Blade Speed Ratio	33	13	7	6	6
Nozzle Inefficiency	21	10	11	11	11
Total Losses	77	62	52	33	27
Engine Efficiency	23	38	48	67	73
Shaft Power Output, kW	33	1265	1587	2208	2415

Notes

*23 nozzles

Shaft output assumes no losses in raw fluid distribution system for full admission.

TABLE 4-5

Resource Utilization Performance Comparisons

	Water rate* lb/kWh (gross)
Total flow impulse turbine system inlet: 2.53 MPa (367 lb/in^2 abs), 14% quality; exit: 13.8 kPa (2 lb/in^2 abs)	
Existing design - full admission extrapolation (38 - 48% efficiencies)	69 - 87
Advanced design - full admission (70% efficiency)#	47
Other systems (calculated for same test conditions)	
Single flash (75% turbine efficiencies)	70
Double flash (77%, 78% HP and LP turbine efficiencies)	54
Helical rotor expander (50% efficiencies with atmospheric exhaust)	110

*Pure water

#Turbine engine efficiencies are quoted

Performance Potential of the Impulse Turbine

In summary, considerable improvement can be expected in turbine performance as a result of droplet size reduction. The performance indicated for droplets smaller than 1 micron also requires that sufficient two-dimensional analytical methods are developed to improve two-phase blade and nozzle design. Indeed, it appears possible to achieve the research goal of 70 percent engine efficiency for the machine. Using the test conditions (Table 4-3) as representative, a 70 percent engine efficiency converts to a resource utilization rate (water rate) for pure water of 21 kg/kWh (47 lb/kWh) gross, i.e. exclusive of the parasitic loads which would occur in a typical power plant application. This represents a significant improvement over conventional conversion systems operating with the same conditions. The important implication is that the number of wells required for a given power output is correspondingly reduced, which in turn, reduces the initial capital investment since the cost of wells is dominant.

The present state-of-the art for the impulse turbine is already competitive with existing systems (Table 4-5). The 38-48% engine efficiency, obtained from the test results, converts to 87-69 lb/kWh respectively. Also, preliminary cost estimates indicate that a 2 MWe total flow system, including condensing and cooling, and fabricated from brine-tolerant materials, would cost about 750 $/kW. This is clearly already competitive with conventional systems which generally are estimated to cost about 800 $/kW for 50 MWe sizes. Even without significant improvements in design, performance, and fabrication methods for production, the total flow impulse turbine is already competitive if the economics of geometric scaling are considered.

4.4.3.3 Comparison of Total Flow Expanders

In order to achieve their highest efficiencies, all expanders must be designed uniquely for site specific conditions. Hence, it is not possible to provide a detailed comprehensive comparison of all candidate expanders to provide a general assessment. Each resource type will likely require a special conversion system or combination of systems (hybrids). It is instructive, however, to estimate the spectrum of relative sizes to produce a nominal 10 MWe (gross) from the range of wellhead conditions listed in Table 4-1. Fig. 4-19 summarizes calculations (House, 1976) comparing the single stage axial flow impulse turbine with a single stage helical rotor expander. Both machines are required to exhaust at 49°C (3.5" Hg), condensing temperature, and both are assumed to have 70% engine efficiencies, even though this may be optimistic for the helical rotor expander. Rotor or wheel diameter D is arbitrarily chosen as the size criterion. This is not entirely useful since the positive displacement devices will likely have lengths greater than the diameters, while the impulse turbine wheel width is very much less than its diameter.

Fig. 4-19 gives approximate diameter ranges as shown. These simple comparisons clearly indicate the size advantage of the impulse turbine. Although no comprehensive system study has yet been made, these results give some idea of relative machine sizes and, implicitly at least, give an indication of relative costs to be expected. Again, it should be emphasized that such a single parameter comparison must be viewed with caution. Site specific conditions, requirement for hybrid systems or combinations of expanders, and specialized applications will be important factors influencing the ultimate choice of expanders. Nevertheless, the size advantege of the impulse device is a major consideration along with its relative mechanical simplicity.

It should be mentioned that the helical rotor expander size could be reduced by accepting a loss in efficiency for a smaller size undergoing an incomplete expansion.

4.4.4 Brine Chemistry Effects

Even though this chapter is limited to discussion of energy conversion concepts, it would not be complete without some reference to the ability of the engines under review to withstand the hostile environment produced by operation on the high salinity geothermal brines. As previously noted, the helical rotor expander has an inherent feature for self-removal of scale, and the relatively low fluid velocities through the machine serve to reduce problems of erosion of the rotors. The impulse turbine, because of high fluid velocities across the blades, will require special materials for erosion resistance. Since all of the pressure (and temperature) drop occurs in the nozzle, a non-rotating component, there are several opportunities for scale control, such as keeping the nozzle wall hot, periodic flexing, "porous" nozzles for boundary layer control, chemical treatment of the brine to inhibit silica precipitation, and use of polymeric liners.

Considerable work has been completed toward field testing methods for scale control and materials evaluation for corrosion/erosion resistance (Tardiff, 1977). We have established that scale deposition can be eliminated by acidification. Dropping the pH value from 5.6 at the wellhead to below 4.5 by addition of about 100 to 200 ppm of hydrochloric acid completely eliminates scaling of nozzles when brine is expanding from wellhead (about 220°C) to atmospheric conditions. Post-test examination of sectioned nozzles subjected to treated and untreated brine showed that control nozzles scaled at a rate of about 0.25 mm/h, while other test nozzles remained clean when exposed to acidified brine. A rough cost analysis shows that acidification

by HCl will add less than 2 mils/kWh to the cost of energy, indicating that the method will likely prove economically feasible as well. Also, experimental evidence now exists that acidification delays the formation of and stabilizes the colloidal suspension of silica in the cooled brine. Thus, plugging of reinjection wells by normally occurring suspended solids might be avoided.

In addition, concurrent tests of turbine blade materials subjected to the high velocity acidified brine streams leaving from the test nozzles indicate that titanium alloys, particularly Ti-6Al-4V, are corrosion/erosion resistant. Although test durations were generally less than 100 h, the results are encouraging. The reader is referred to Chapter 6 for a detailed discussion of the problems involved in brine utilization.

4.4.5 A Possible Total Flow System

Although there are not yet precise indicators of the outcome of current development efforts, it is likely that each machine will find a unique place. The present view is that the Total Flow Process will, however, emerge as a reality in some form. One possible system utilizing the impulse turbine is shown in Fig. 4-20 which is an artist's conception synthesizing the technical facts currently available. The basic element is a horizontal axial flow turbine wheel fed by fluid passing through nozzles spaced around the periphery. Condensing would be accomplished by a modified barometric condenser designed to separate the vapor fraction from the liquid in order to isolate the cooling system.

The significant concludion is that the recent test data on turbine performance, the field tests on scale control, and the promising results on material-tests all indicate that the Total Flow Concept has moved from a far-out to a near-term technology for geothermal applications. Although much more work needs to be done to establish performance limits and

reliability, it can be clearly concluded that technical feasibility is established, the key technical issues are clear, strategies for development are defined, and the economics of the concept are promising.

The above discussion has emphasized technical aspects and no attempt has been made to produce explicit economic evaluations. Future costs, material availability and financial factors are speculative at the time of writing. Reliable economic analysis requires design data and proven system components which do not yet exist.

4.4.6 References

Alger, T., "The Performance of Two-Phase Nozzles for Total Flow Geothermal Impulse Turbines", Presented at the 2nd U.N. Symposium on Development and Use of Geothermal Resources, San Francisco, CA, May 20-29, 1975.

Alger, T., unpublished data, private communication, 1976.

Austin, A. L., G. H. Higgins, and J. H. Howard, "The Total Flow Concept for Recovery of Energy from Geothermal Hot Brine Deposits", Lawrence Livermore Laboratory, UCRL-51366, April, 1973.

Comfort, W., T. Alger, W. Giedt, W. Crowe, "Calculation of Two Phase Dispersed Droplet-in-Vapor Flows Including Normal Shocks", LLL Report UCRL-78426, July, 1976, Also presented at the ASME Winter Annual Meeting, NY, December, 1976.

Comfort, W., "Interim Report on Performance Tests of a Total Flow Impulse Turbine for Geothermal Applications", LLL report, UCID 17411, March, 1977. Also: Intersociety Energy Conversion Conf., 1977.

Comfort, W. J., "The Design and Evaluation of a Two-Phase Turbine for Low Quality Steam-Water Mixtures," Lawrence Livermore Laboratory, UCRL 52281, May, 1977.

Elliott, D., "Comparison of Brine Production Methods and Conversion Processes for Geothermal Electric Power Production", EQL #10, July, 1975. Environmental Quality Laboratory, Pasadena, CA.

Facca, G., "The Structure and Behavior of Geothermal Fields", Geothermal Energy, Edited by C. H. Armstead, UNESCO, Paris, 1973, pp. 61-69.

Gould, T. L., "Vertical Two-Phase Steam-Water Flow in Geothermal Wells", Jour. Pet. Tech., August, 1974, pp. 833-842.

Grens, J. Z., "Effects of Salinity on Geothermal Well Performance, LLL Report UCID-16791, May, 1975.

House, P. A., "Helical Rotor Expander Applications for Geothermal Conversion", LLL Report UCRL-52043, April, 1976.

James, R., "Optimum Wellhead Pressure for Geothermal Power, New Zealand Engineering, V. 22, p. 221 (1967).

James, R., "Factors Controlling Borehole Performance", Geothermics (1970) Special Issue 2, p. 1502.

James, R., "Power Station Strategy", Geothermics (1970) Special Issue 2, p. 1676-1687.

Johnson, P., "Model to Calculate Flow and Energy from Geothermal Wells", LLL Internal Engr. Note ENE 74-9, April 5, 1974.

McKay, R. A. and R. S. Sprankle, "Helical Rotary Screw Expander Power System", Conf. on Res. for Dev. of Geothermal Energy Resources, Sponsored by NSF, Rept. NSF-RA-N-74-159, Pasadena, Sept. 23-25, 1974, pp. 301-309.

Muffler, J. J. P., and D. E. White, "Geothermal Energy", The Science Teacher, V. 39, No. 3, pp. 1-4 (1972).

Naymanov, O. S., "A Pilot Geothermoelectric Power Station in Pauzhetka, Kamachatka", Geothermics (1970), Special Issue #2, Vo. 2, part 2, pp. 1563-1564.

Possell, C. R., "Bladeless Turbines as a Geothermal Prime Mover and Potential Reinjection Pump", Presentation to Symp. on "New Sources of Energy", Univ. So. Cal., May 9, 1973, (General Ener-Tech., San Diego, CA).

Rice, W., Dept. of Mech. Engr., Ariz. State Univ., Tempe, AZ.

Steidel, R. F., Jr., H. Weiss, and J. E. Flower, "Performance Characteristics of the Lysholm Engine as Tested for Geothermal Power Applications in the Imperial Valley", LLL, UCRL-80151, August, 1977.

Tardiff, G., "Chemistry and Materials Technology for Utilization of High-Salinity Brines", LLL, Intersociety Energy Conversion Conf., Washington, D.C., 1977.

Weiss, H., and G. Shaw, "Geothermal Two-Phase Test Facility", Presented at the Second U.N. Symp. on Dev. and Use of Geothermal Resources, San Francisco, CA, May 20-29, 1975.

Weiss, H., R. F. Steidel, and A. Lundberg, "Performance Test of a Lysholm Engine", LLL Report UCRL-51861, July 3, 1975.

White, D. E., "Characteristics of Geothermal Resources", Geothermal Energy, Edited by P. Kruger, and C. Otte, Stanford Univ. Press, 1973, pp. 69-95.

Bibliography

Austin, A. L. and A. W. Lundberg, "A Comparison of Methods for Electric Power Generation from Geothermal Hot Water Deposits", Preprint 76-WA/ENER-10, Presented at Winter Annual Meeting of the ASME, NY, November 17-22, 1974.

Beaulaurier, L. O., "Binary Thermodynamic Power Cycles Applied to Geothermal Fluids", Bechtel Corp., San Francisco, CA, Paper presented at the First Geothermal Implementation Conf., Wairakai, New Zealand, May, 1974.

Crowe, C. T., "Conversion Equations for Vapor-Droplet Flows Including Boundary Droplet Effects", LLL Report UCRL-52184, December, 1976.

Hinrichs, T. C., San Diego Gas and Electric Co., "Imperial Valley Geothermal Activities - A Status Report", Conf. on Res. for the Development of Geothermal Energy Resources, Sponsored by NSF, Rept. NSF-RAN-159, Sept. 23-25, 1974, pp. 194-206.

Kuwada, J. T., "Geothermal Power Plant Design", AICHe Symp. Series, No. 129, V. 69 (1972), pp. 439-444.

Moskvicheva, V. N. and A. E. Popov, "Geothermal Power Plant on the Paratunka River", Geothermics (1970), Special Issue #2, pp. 1562-1571.

Wehlage, E. F., Geothermal Energy, April, 1974, p. 6-12.

GLOSSARY

Total Flow Concept - The attempt to expand in equilibrium a low-quality two-phase liquid/vapor mixture over the full pressure/temperature range available in order to secure the maximum possible ("total") enthalpy drop of the mixture. (4.4.3)

Flashed Steam - Steam formed as a result of pressure reduction of boiling water. The steam may be expanded for power. The residual water may be further "flashed" or rejected. (4.4.3)

Binary Cycle - A system employing two distinct working fluids, e.g. water and isobutane, each undergoing its independent work-producing cycle and contributing to the total output. (4.4.2)

Quality (or dryness fraction) - The proportion of vapor in unit mass of a saturated liquid/vapor mixture. Mass proportions are generally employed.

Monodisperse - Refers to a dispersion in which all the bubbles, drops or particles are equal in size. (4.4.3.2)

Velocity Coefficient - The nozzle velocity coefficient is defined as the ratio of the Actual Exit Velocity/Velocity after Isentropic Expansion. (4.4.3.2)

Homogeneous Two-Phase Flow - This term is employed when both liquid and vapor phases flow together without relative velocity, i.e., there is no "slip".

Positive Displacement Expander - A machine in which "displacement" work is done by the working fluid as it enlarges its volume by displacing a piston, rotor vane, etc., which transmits the work to the output shaft. The principle is different from that of the turbine in which the work is done by fluid momentum change in the moving blades. (4.4.3.2)

The following terms refer to the turbine. (4.4.3.2)

Full Admission - A turbine has full admission when the working fluid is admitted to the rotor blades around the complete periphery of the wheel. In Partial Admission the admission arc is less than 360°.

Impulse Turbine - A pure impulse turbine is one in which the working fluid enthalpy drop occurs wholly within the fixed (stator) expansion passages, whether blades or nozzles.

Reaction Turbine - A pure reaction turbine is one in which the working fluid enthalpy drop occurs wholly within the moving (rotor) expansion passages whether blades or nozzles.

Turbine Efficiencies

The nozzle efficiency is the ratio of the effective enthalpy drop in the nozzle to the isentropic enthalpy drop.

The turbine (or engine) efficiency is the ratio of the power delivered by the shaft to the power equivalent of the isentropic enthalpy drop.

The blade efficiency is the ratio of the kinetic energy utilized by the blade to the kinetic energy delivered to the blade by the nozzle.

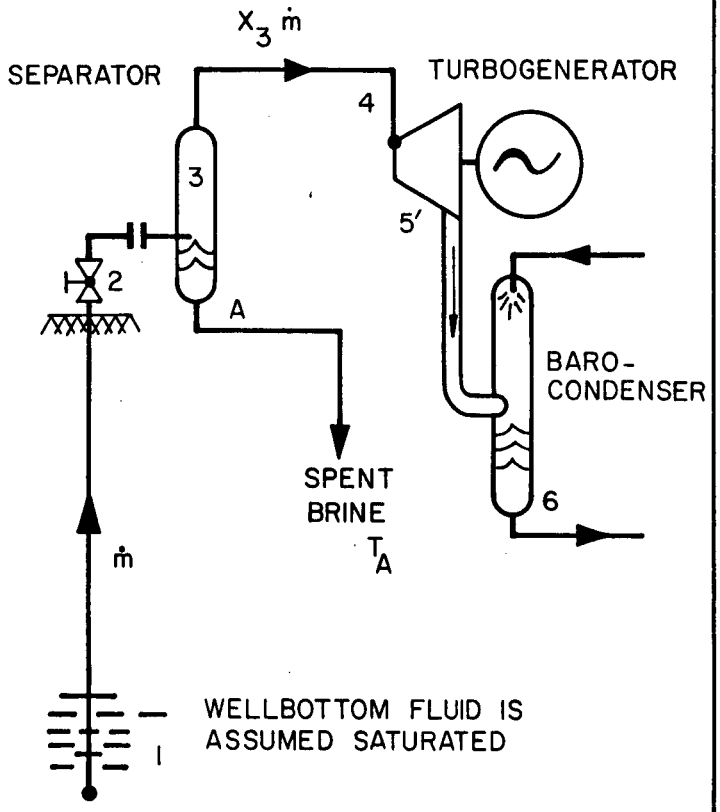

A. SYSTEM COMPONENTS

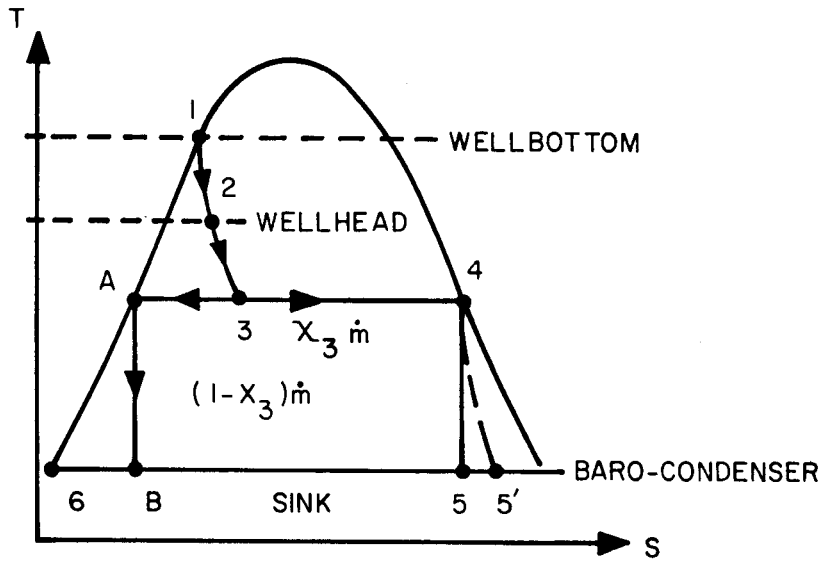

NEGLECTING KINETIC AND POTENTIAL ENERGIES;

NET POWER OUT $= X_3\,\dot{m}\,(h_4 - h_5)\,e_e$

POWER LOST IN SPENT BRINE $= \dot{m}\,(1-X_3)\,(h_A - h_B)$

$$\text{OVERALL THERMAL EFFICIENCY} = \frac{X_3\,(h_4 - h_5)\,e_e}{h_2 - h_6}$$

B. THE PROCESS

FIG. 4-1 THE FLASHED STEAM SYSTEM.

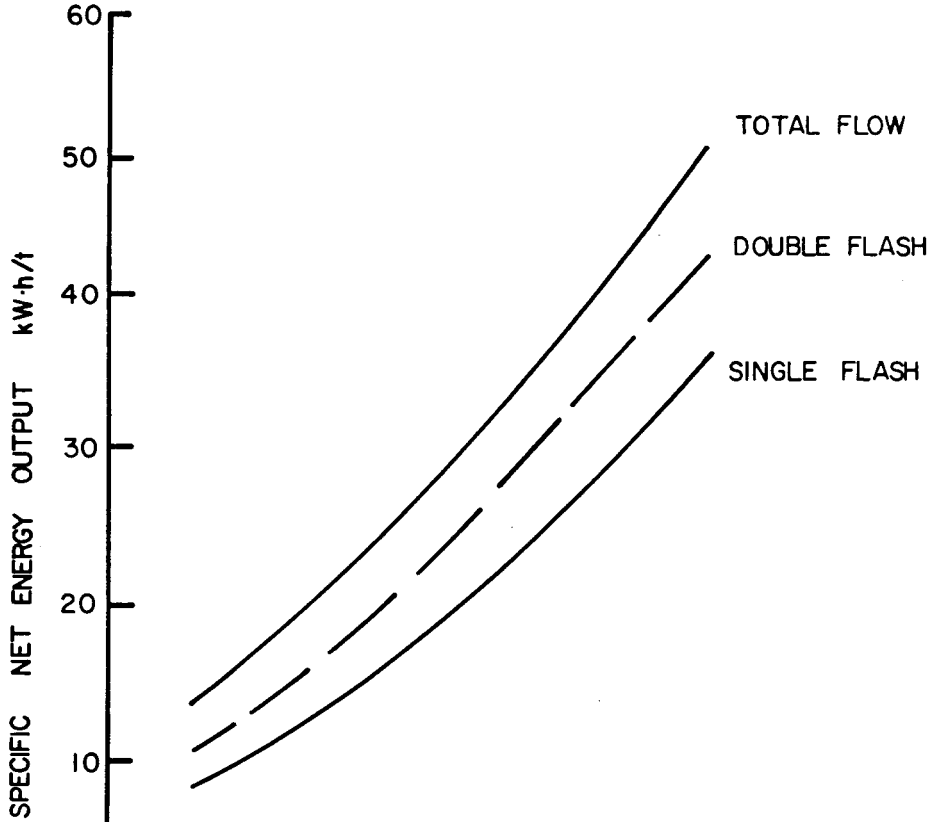

SINGLE FLASH - 75% ENGINE EFFICIENCY
DOUBLE FLASH - 75% ENGINE EFFICIENCY, BOTH STAGES
TOTAL FLOW - 70% EXPANDER EFFICIENCY
ALL SYSTEMS ASSUMED TO HAVE 10% PARASITIC LOSSES
NON-CONDENSIBLES - 0%
CONDENSING TEMP. = 49°C (120°F)
CALCULATIONS BASED ON PROPERTIES OF PURE WATER

FIG. 4-2 PERFORMANCE COMPARISON OF TOTAL FLOW CONCEPT WITH THE FLASHED STEAM SYSTEM.

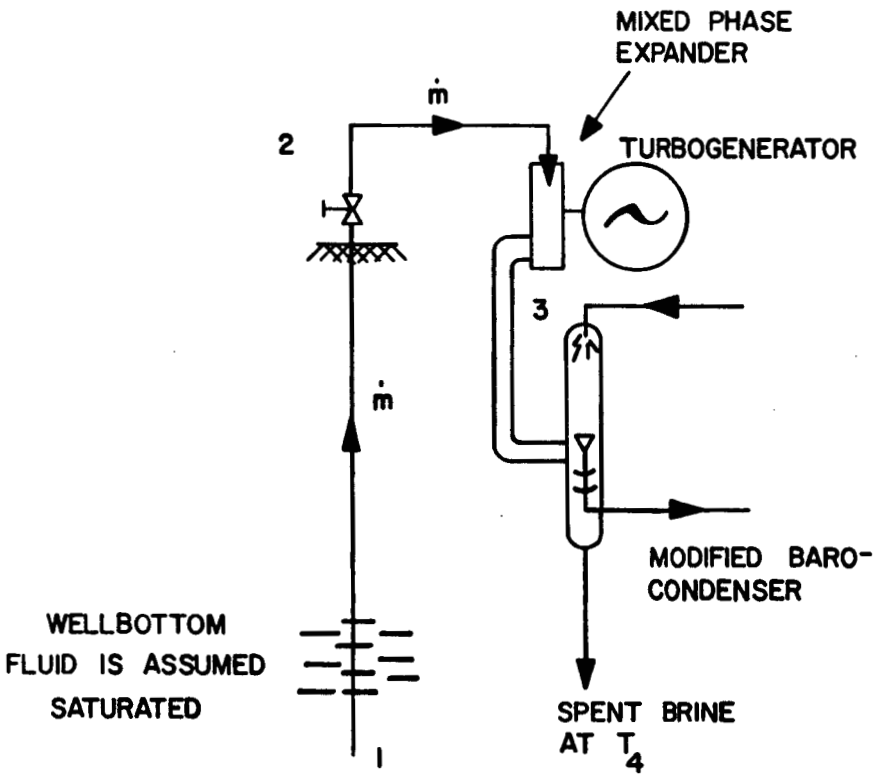

A. SYSTEM COMPONENTS

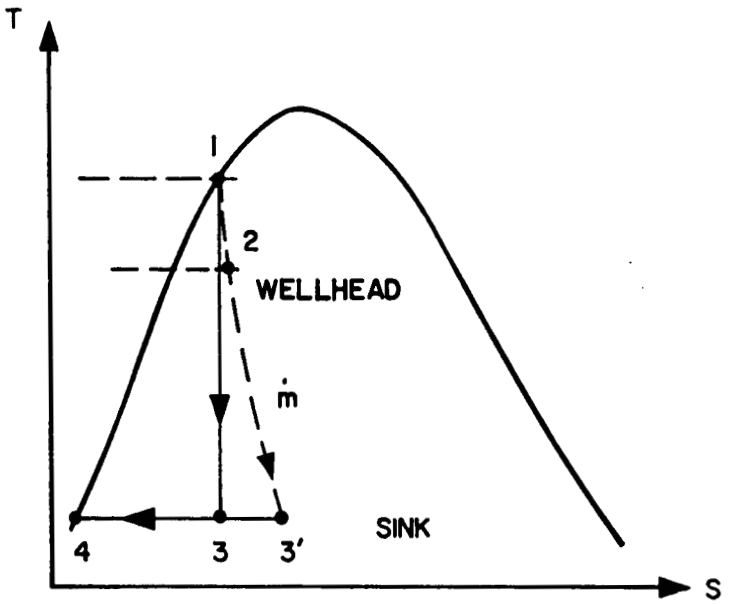

NEGLECTING KINETIC AND POTENTIAL ENERGIES

NET POWER OUT = $\dot{m}(h_2 - h_{3'})\, e_e$

POWER LOST IN SPENT BRINE = 0

OVERALL THERMAL EFFICIENCY = $\left(\frac{h_2 - h_{3'}}{h_2 - h_4}\right)$

B. THE PROCESS

FIG. 4-3 THE TOTAL FLOW CONCEPT

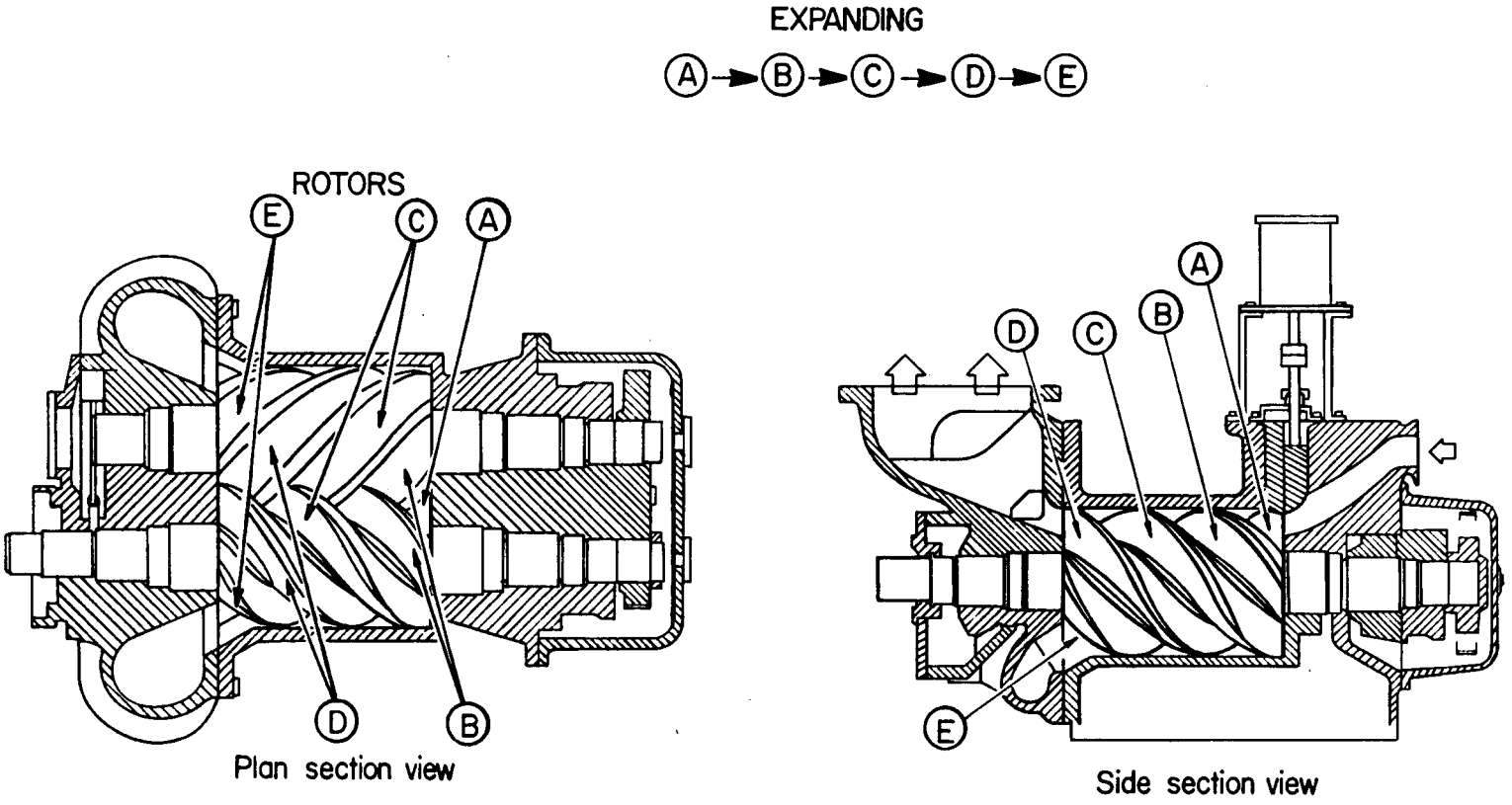

FIG. 4-4 HELICAL ROTOR EXPANDER: The working fluid is admitted at A. The effective passage expands in volume as the fluid traverses the passage in the sequence B-C-D-E.

NEGLECTING KINETIC AND POTENTIAL ENERGIES

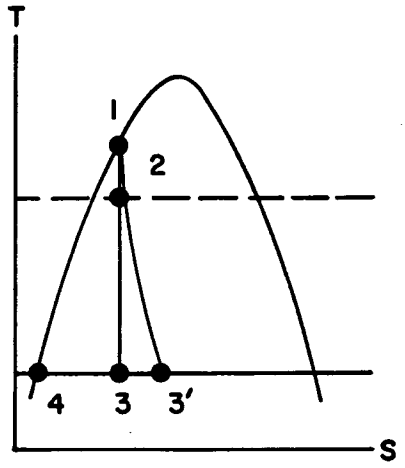

$$\Delta h_s = h_2 - h_3$$

$$V_{3'} = \eta V_3 = \eta \sqrt{2 (h_2 - h_3)}$$

$$\dot{W}_{OUT} = \dot{m} (h_2 - h_3) \eta^2 e_w$$

$$\therefore \eta^2 e_w = e_t$$

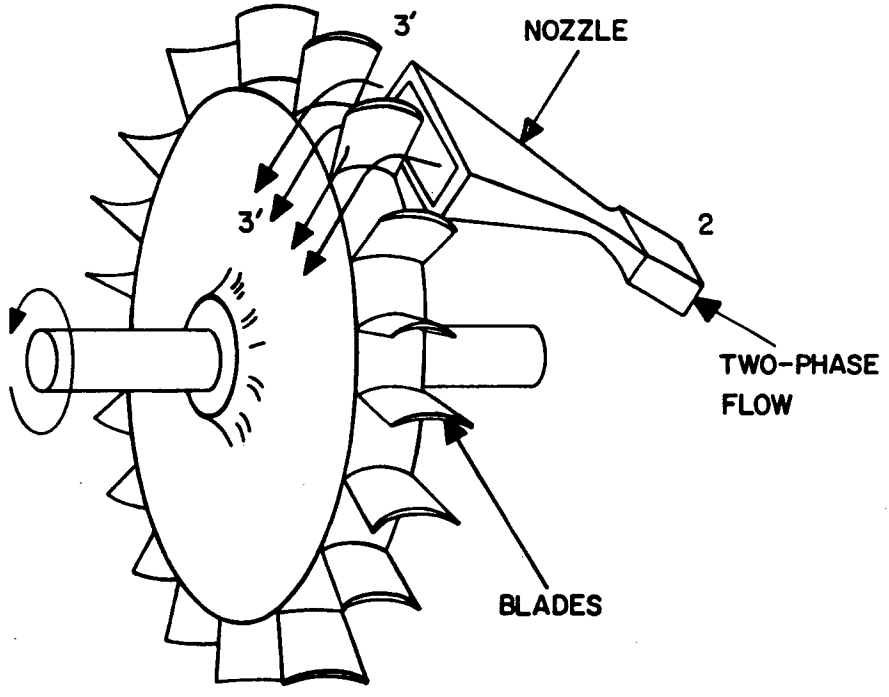

FIG. 4-5 THE AXIAL FLOW IMPULSE TURBINE

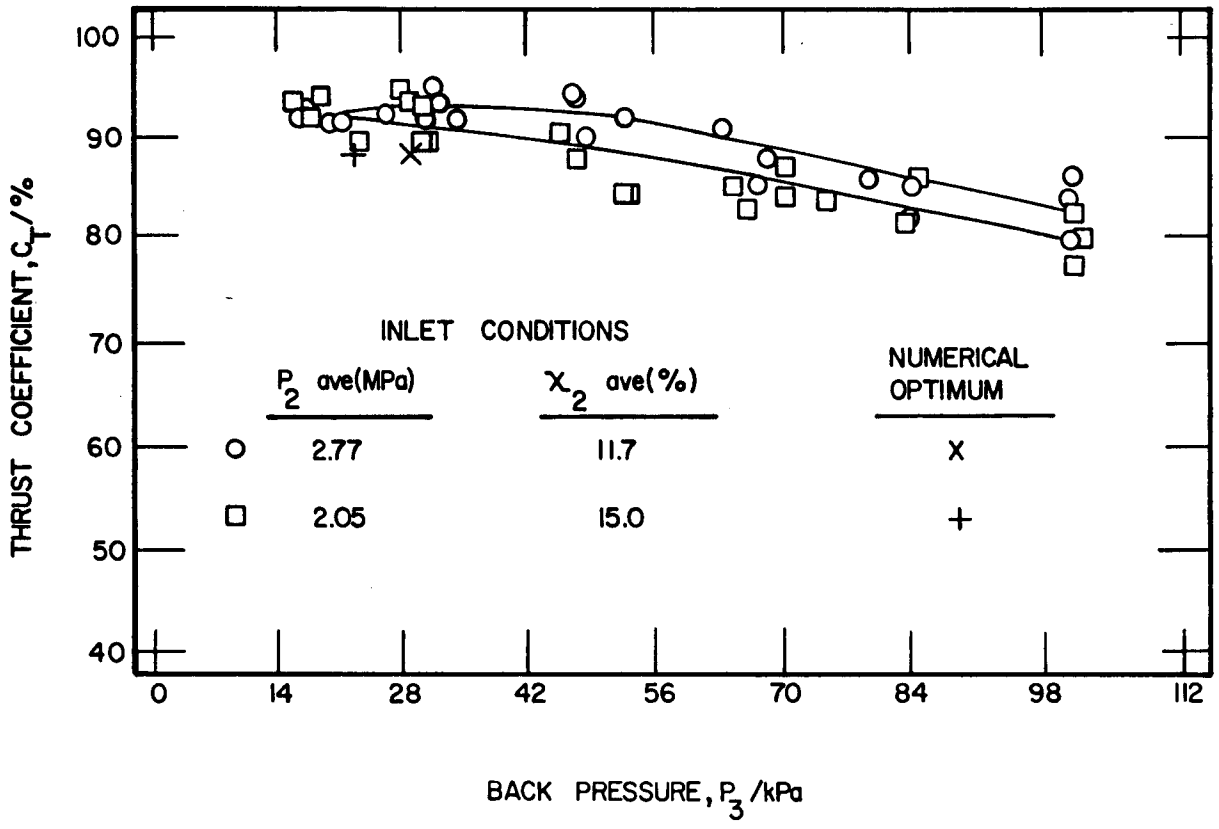

FIG.4-6 THRUST COEFFICIENT DATA AS A FUNCTION OF BACK PRESSURE AND NOZZLE INLET CONDITIONS FOR NOZZLES #2, #3, AND #4.

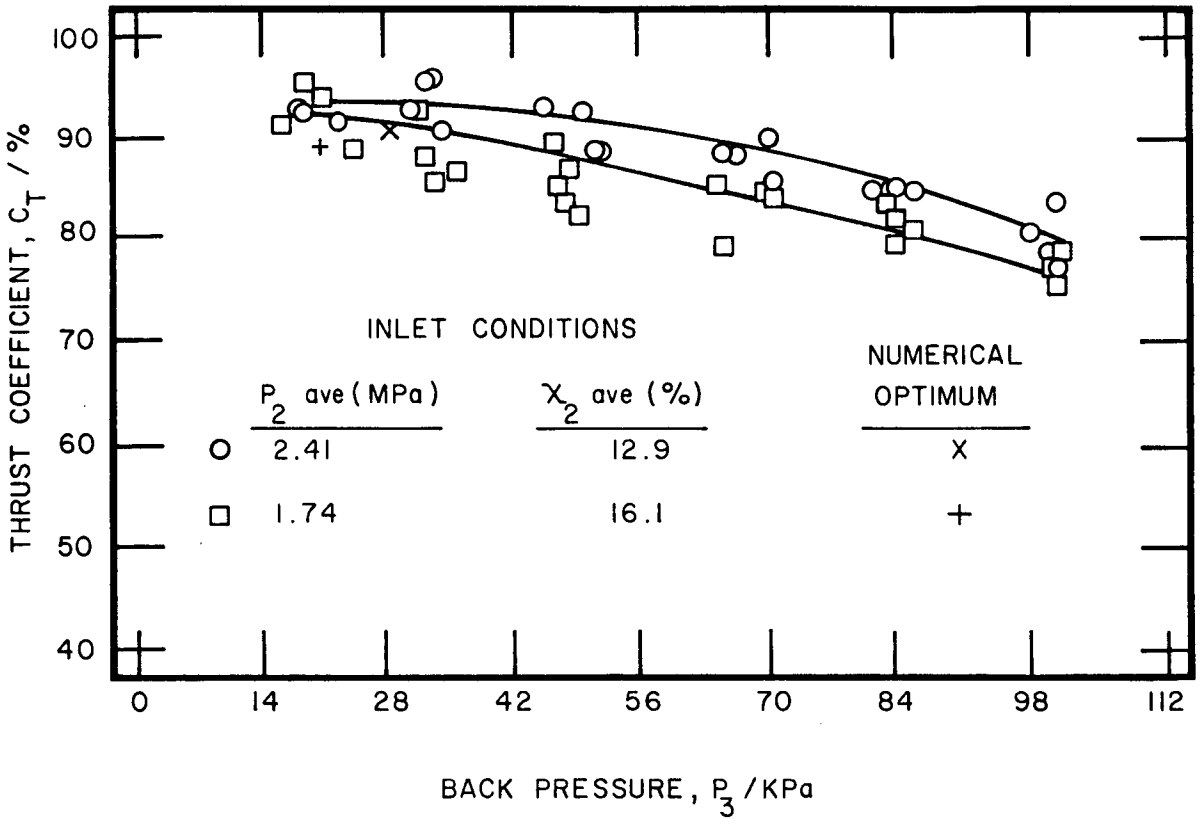

FIG. 4-7. THRUST COEFFICIENT DATA AS A FUNCTION OF BACK PRESSURE AND NOZZLE INLET CONDITIONS FOR NOZZLES #2, #3, AND #4.

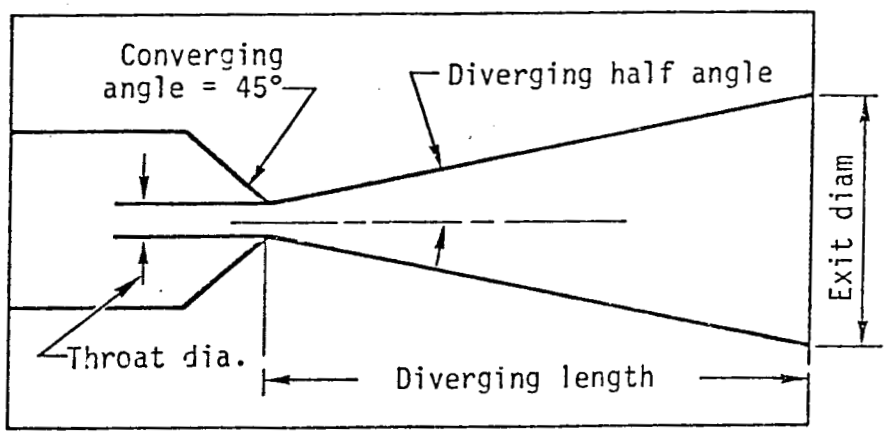

Nozzle	Throat dia. (10^{-3}m)	Exit dia. (10^{-2}m)	Diverging length (10^{-2}m)	Diverging angle(°)
2	6.401	3.183	6.048	12
3	6.401	3.183	8.077	9
4	6.401	3.183	12.129	6
7	9.017	5.664	22.720	6

FIGURE 4-8. NOZZLE NUMERICAL DESIGNATIONS AND DIMENSIONS

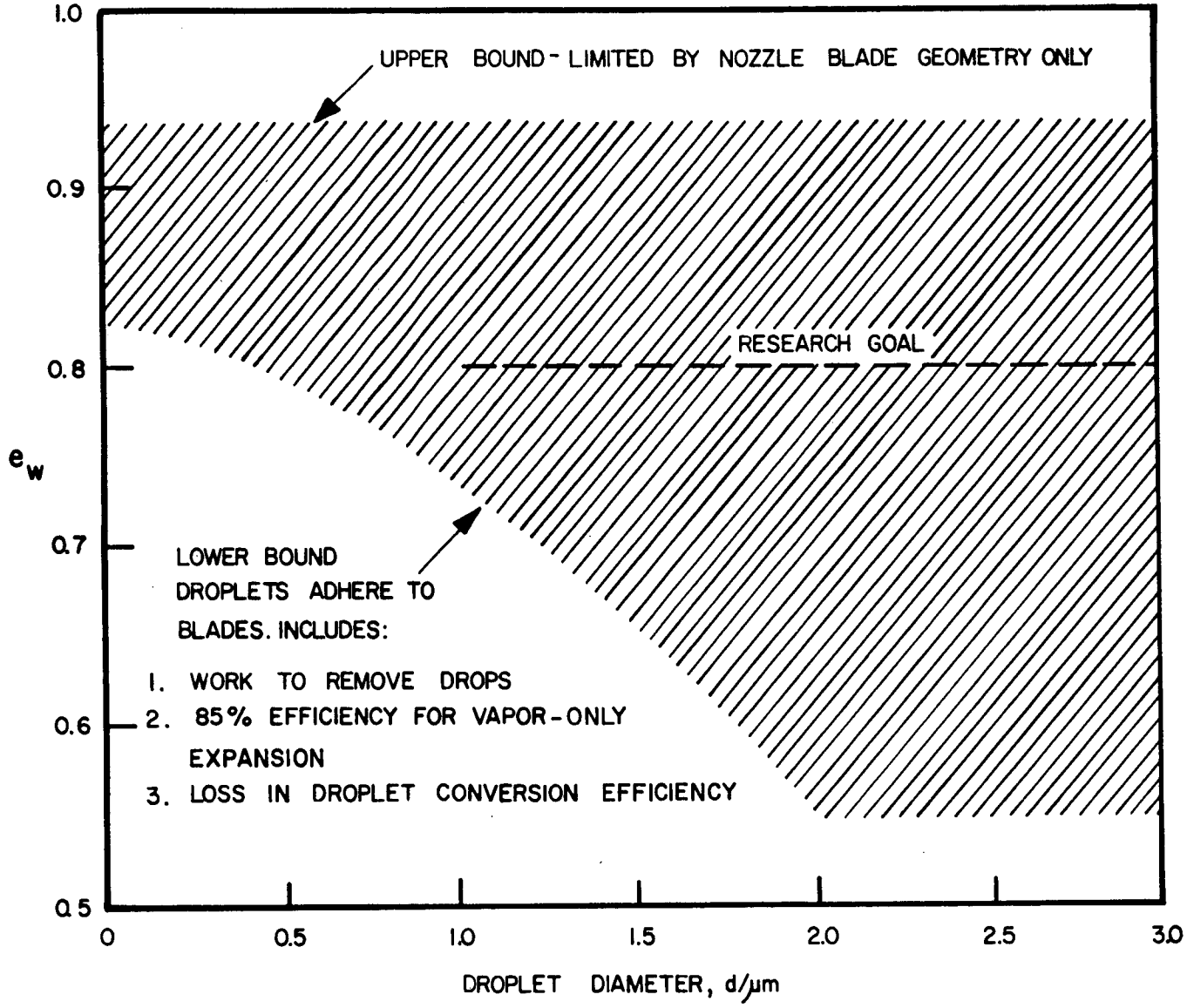

FIG.4-9 ESTIMATED RANGE OF POSSIBLE WHEEL EFFICIENCIES FOR AN AXIAL FLOW IMPULSE TURBINE

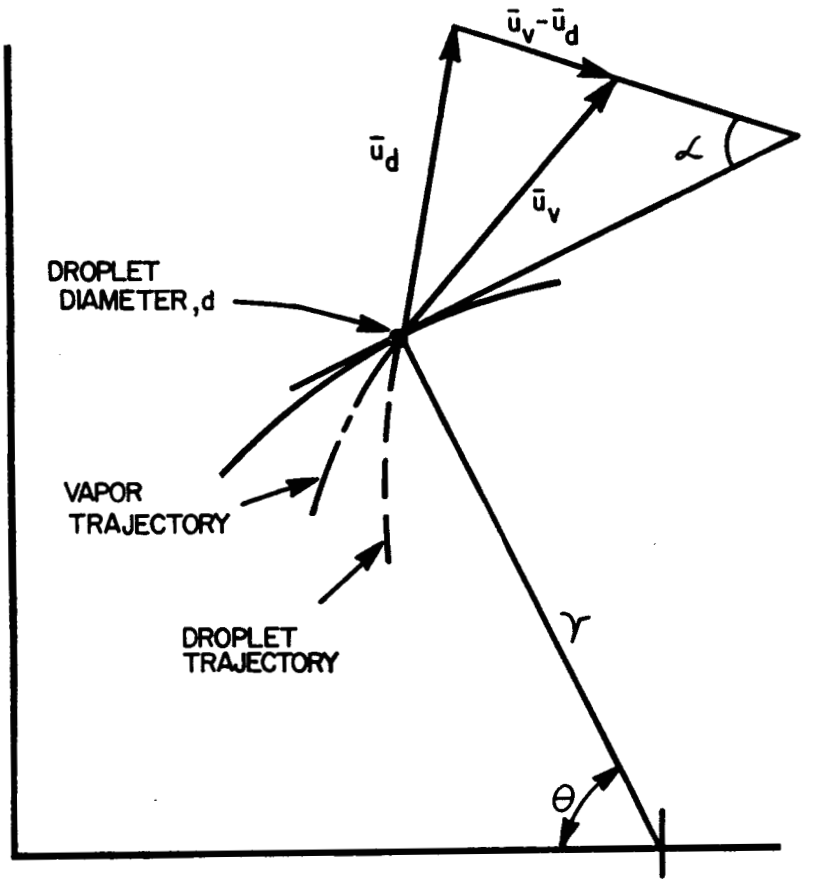

FIG. 4-10 NOTATION FOR DROPLET TRAJECTORY CALCULATIONS

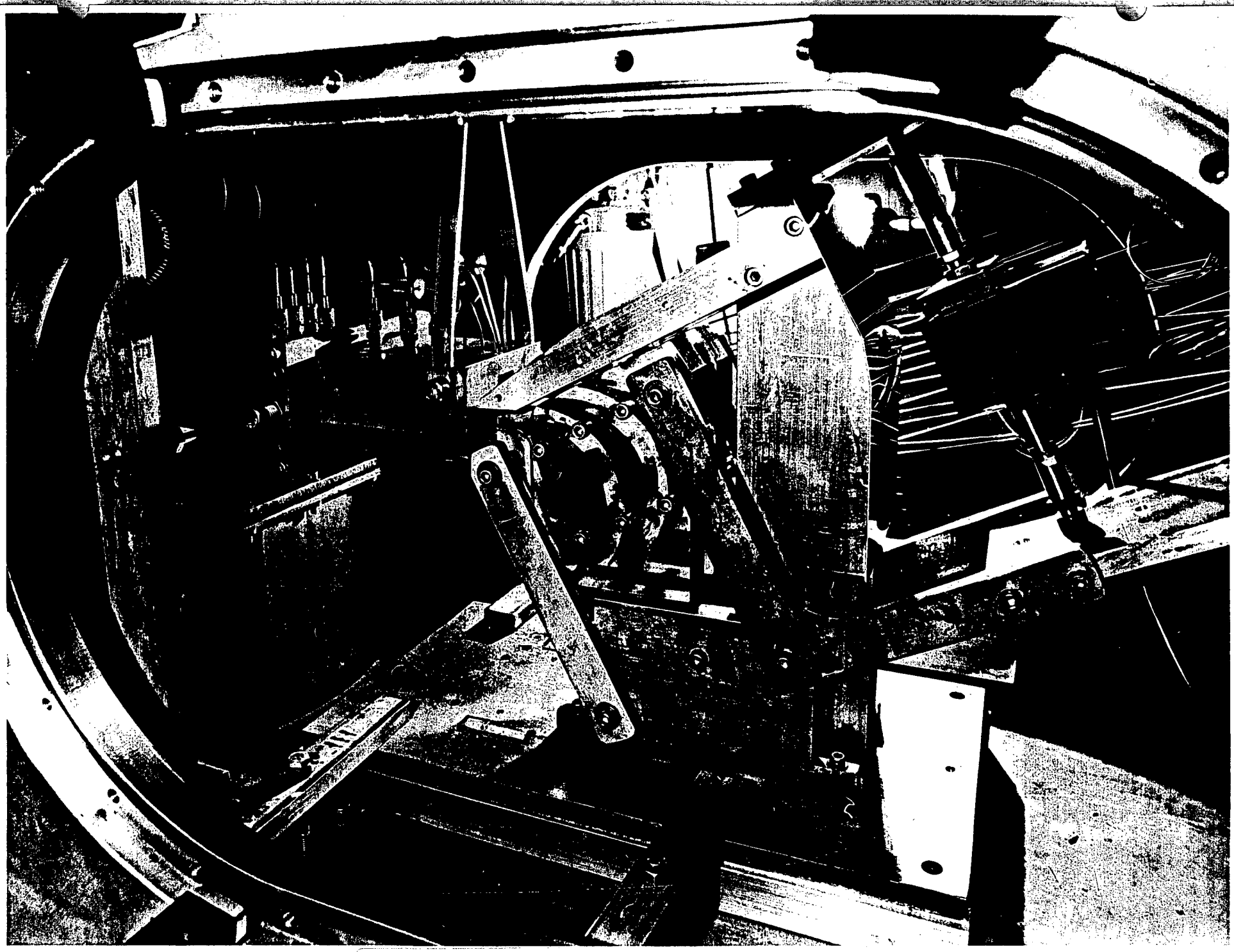

FIGURE 4-11. APPARATUS FOR TESTING BLADE THRUST AND PRESSURE DISTRIBUTION

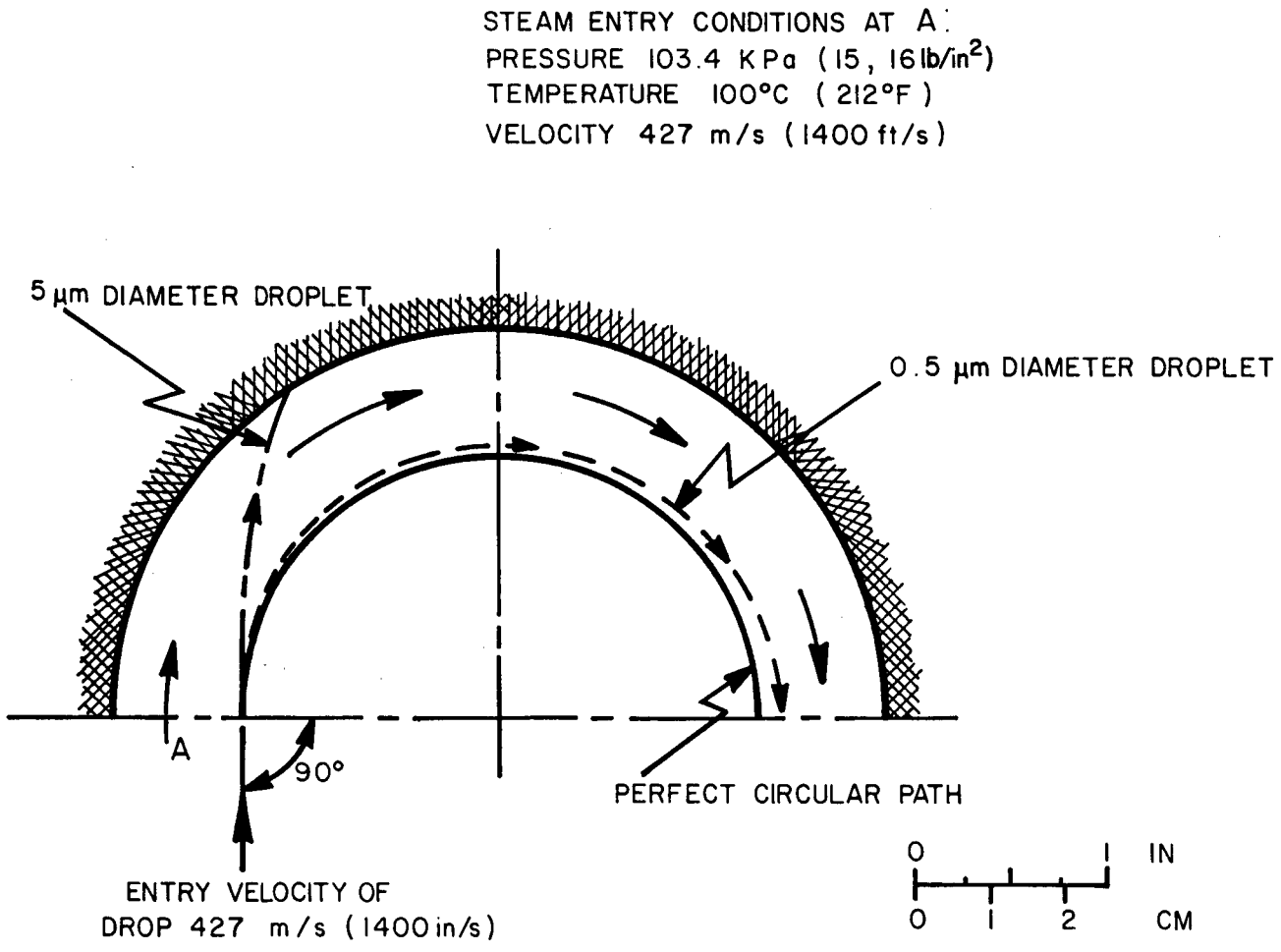

FIG. 4-12 CALCULATED TRAJECTORIES OF DROPLETS TRAVERSING A 180° TURN

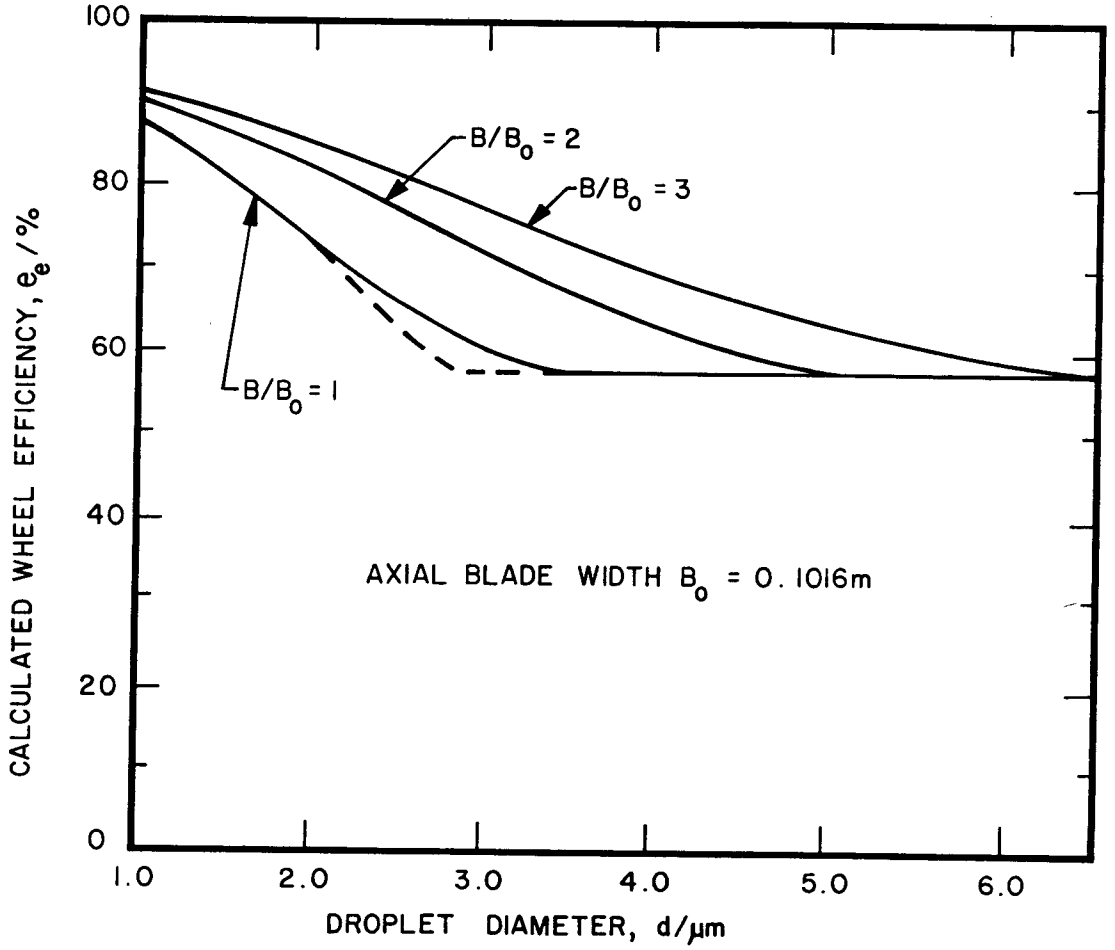

FIG. 4-13 IDEALIZED ROTOR PERFORMANCE AS A FUNCTION OF DROPLET-DIAMETER FOR VARIOUS BLADE WIDTHS.

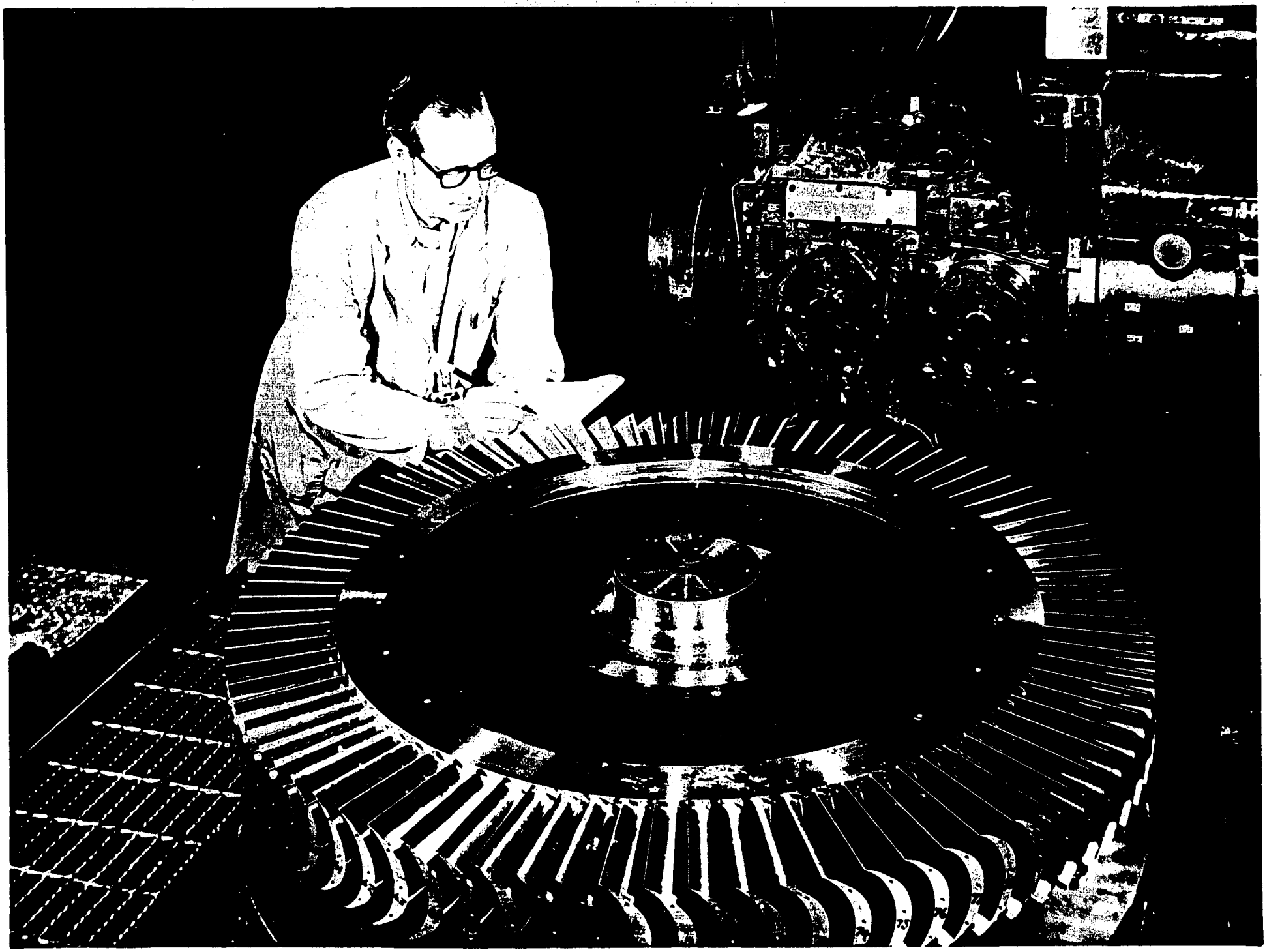

FIGURE 4-14. COMPLETED ROTOR BEFORE PLATING

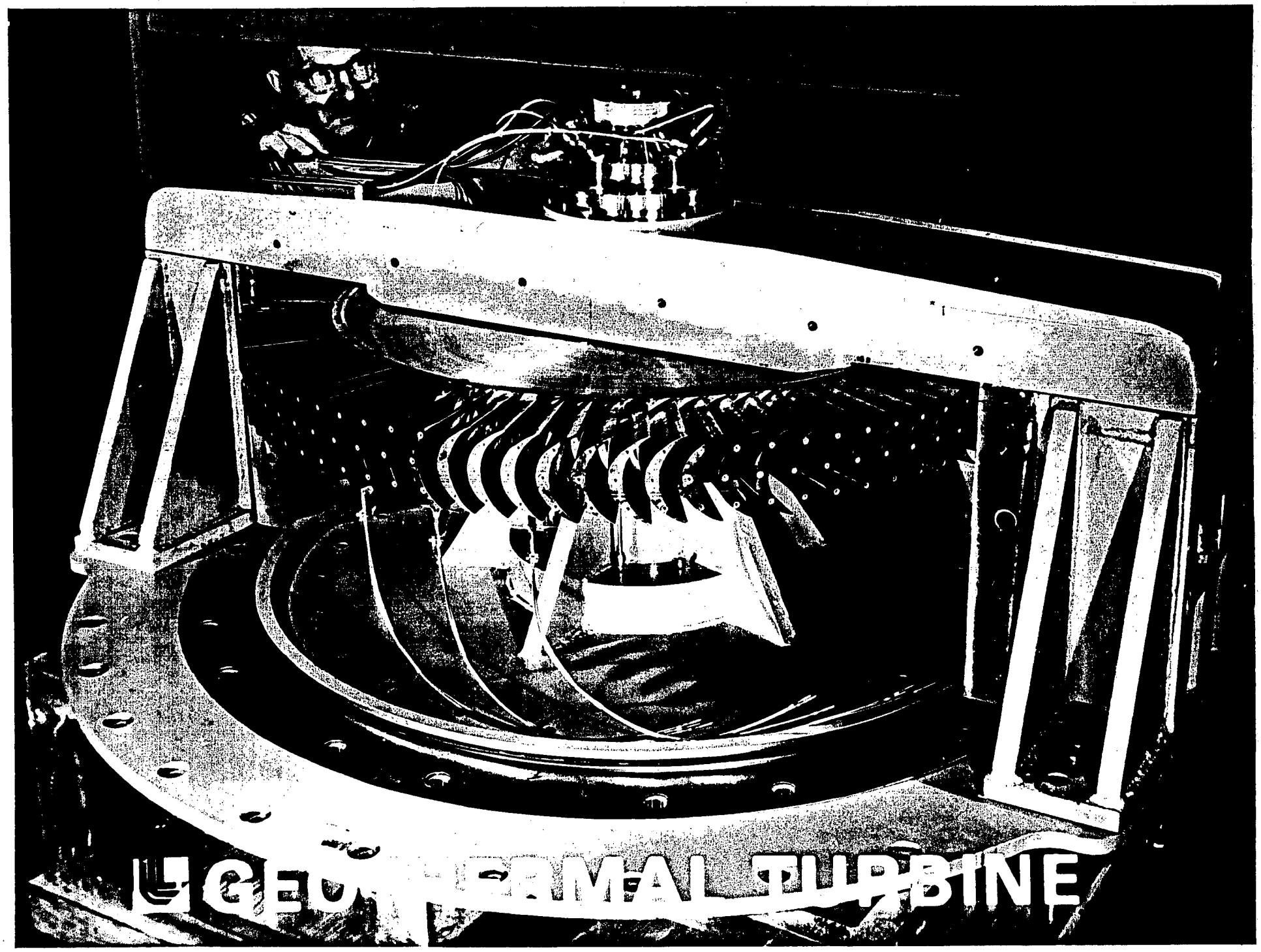

FIGURE 4-15. ASSEMBLY OF ROTOR INTO STATOR

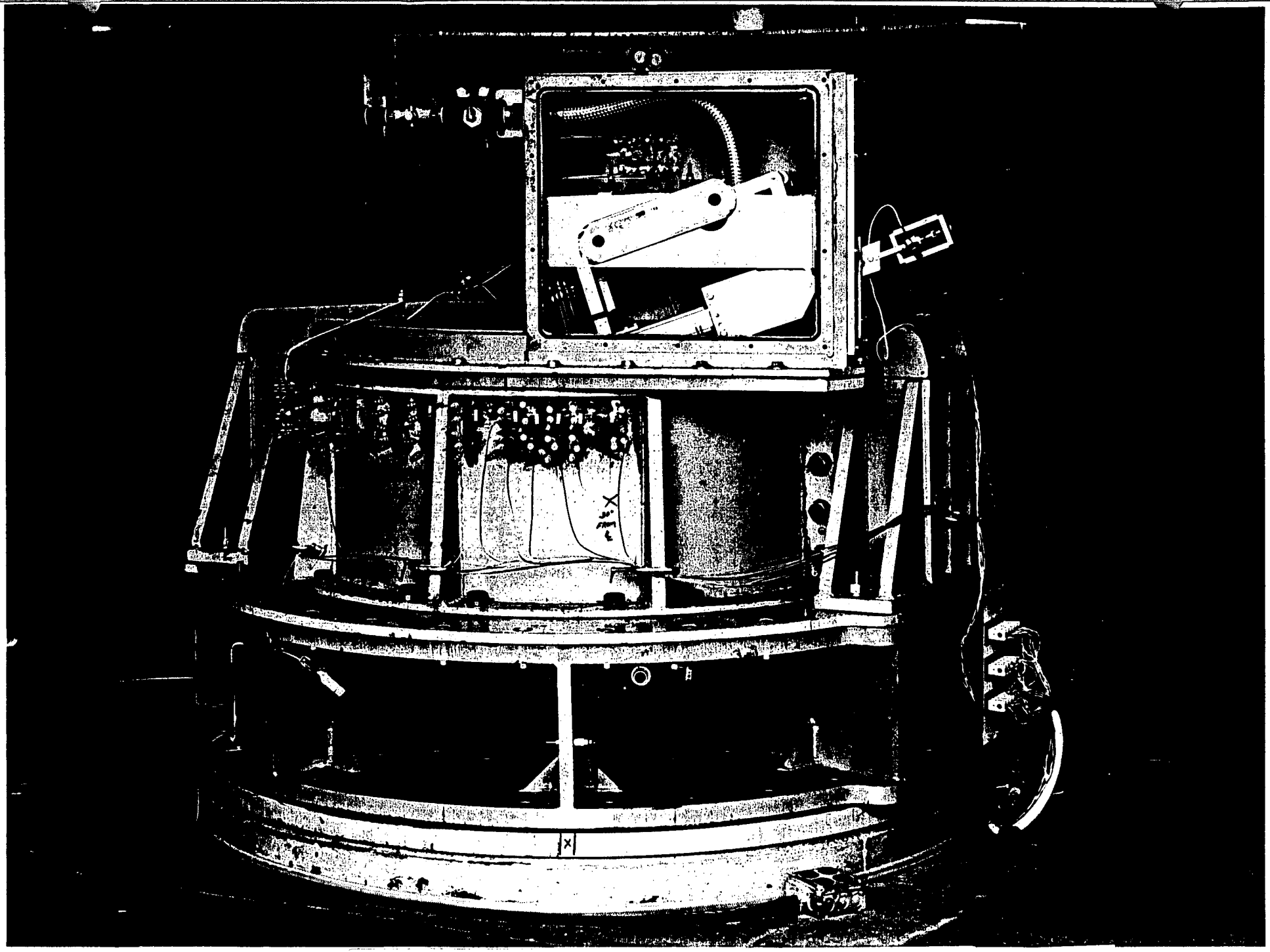

FIGURE 4-16. MEASURING THE NOZZLE AXIAL THRUST DURING PERFORMANCE TESTING OF THE EXPANDER

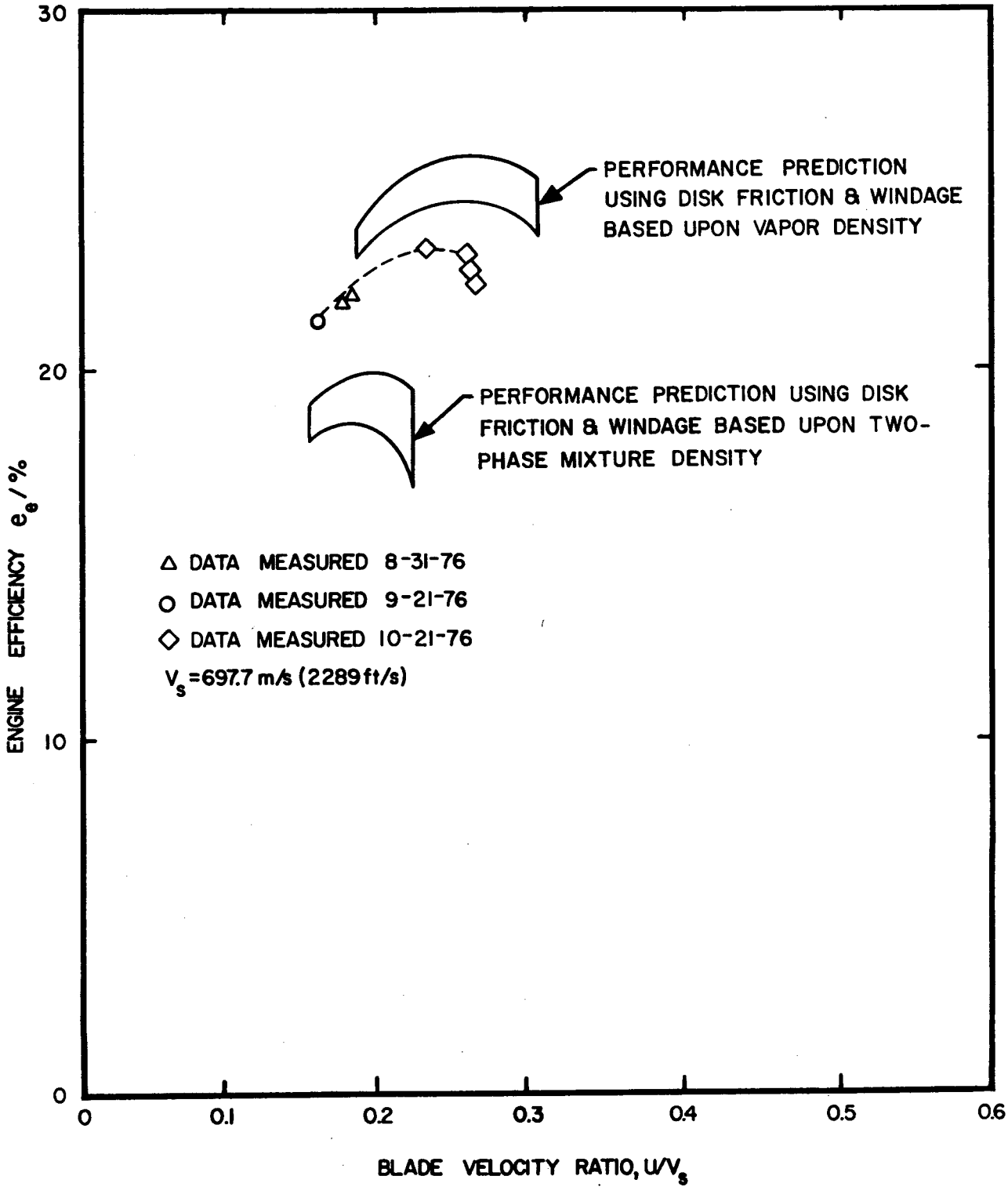

FIG. 4-17 COMPARISION OF EXPERIMENTAL DATA WITH TURBINE PERFORMANCE MODEL PREDICTIONS

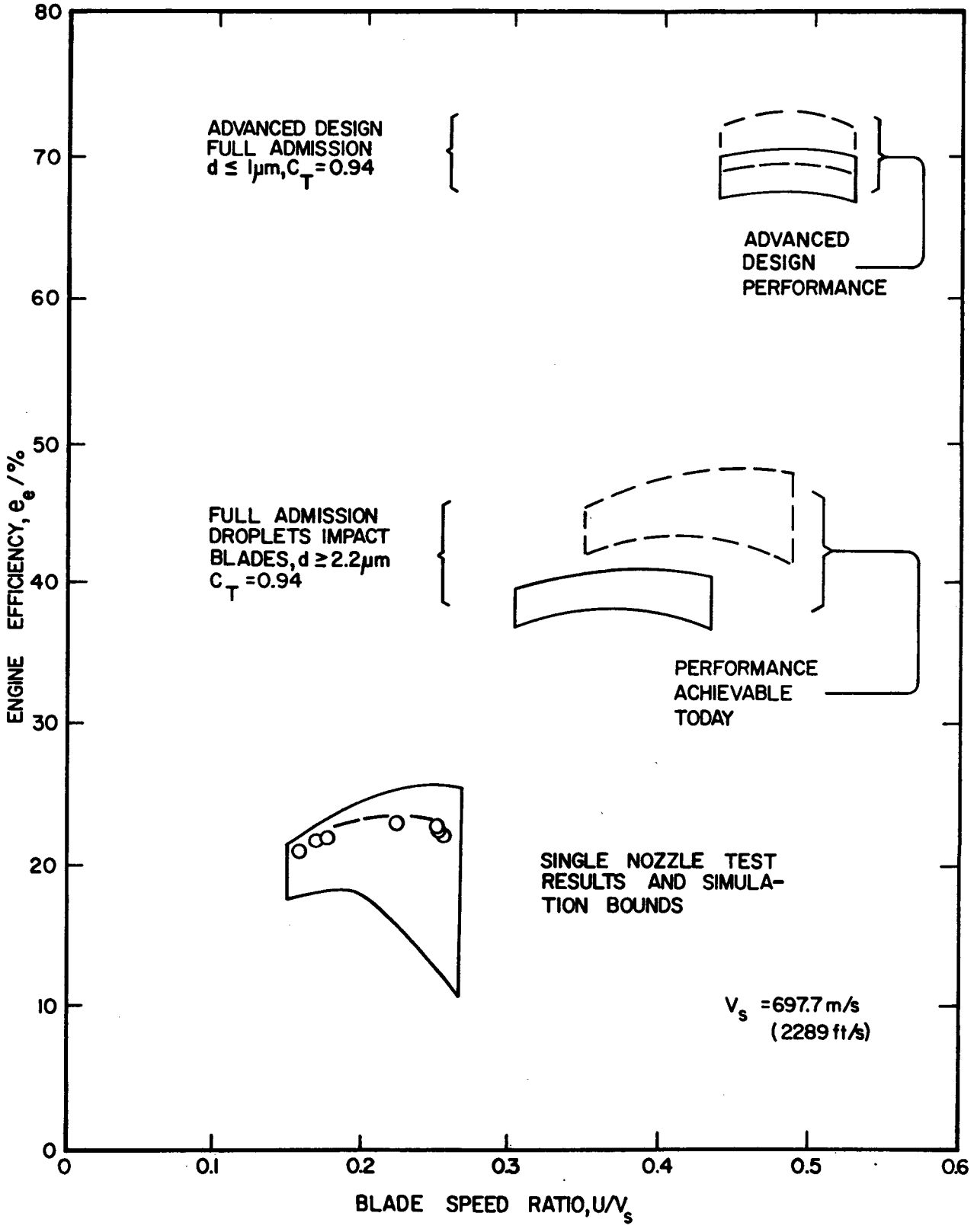

FIG. 4-18 EXTRAPOLATIONS USING THE NUMERICAL PERFORMANCE MODEL

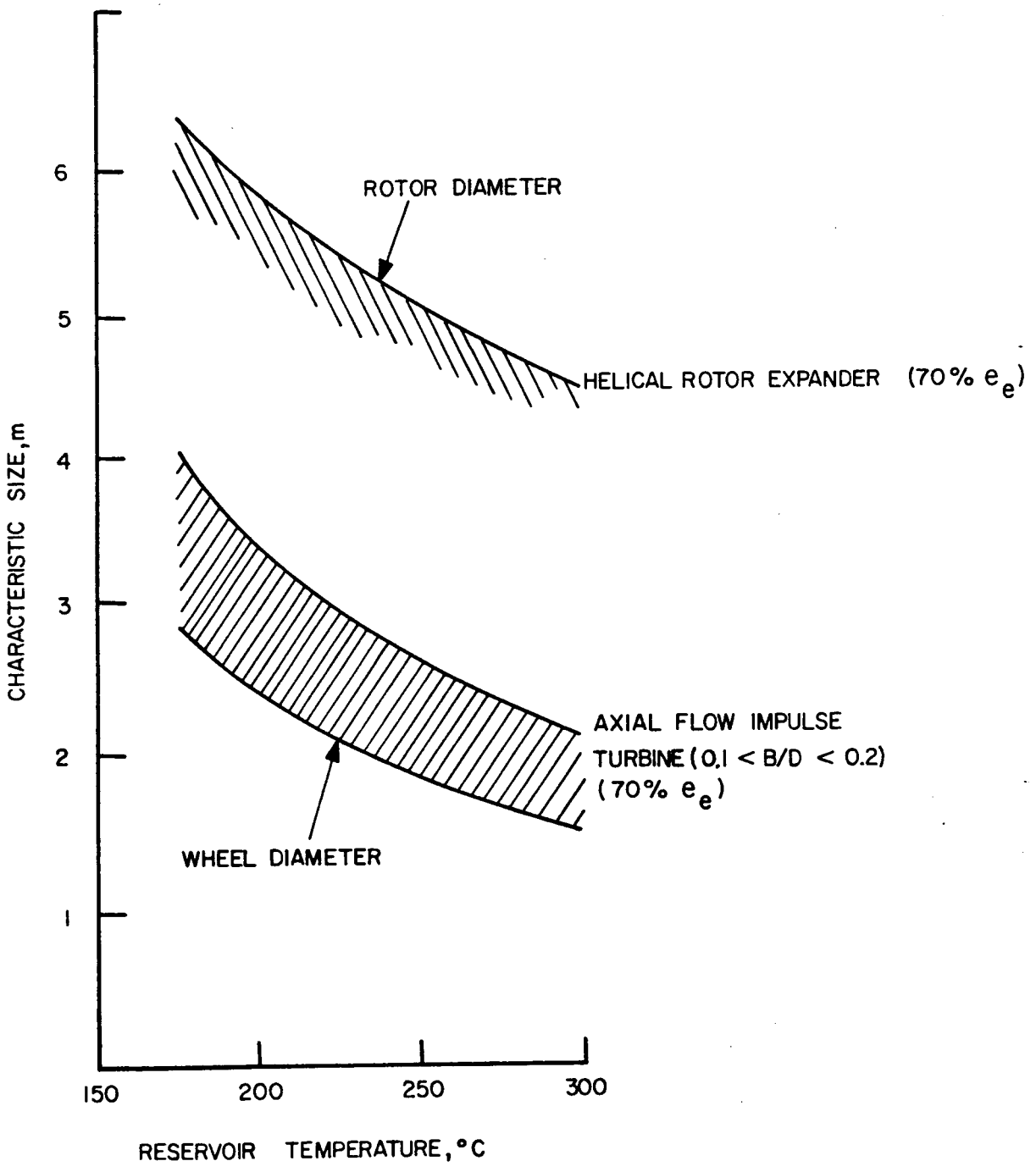

FIG. 4-19 RELATIVE SIZES OF TOTAL FLOW EXPANDERS WORKING TO 49°C (11.9 kPa) SINK CONDITION (10 MW CAPACITY)

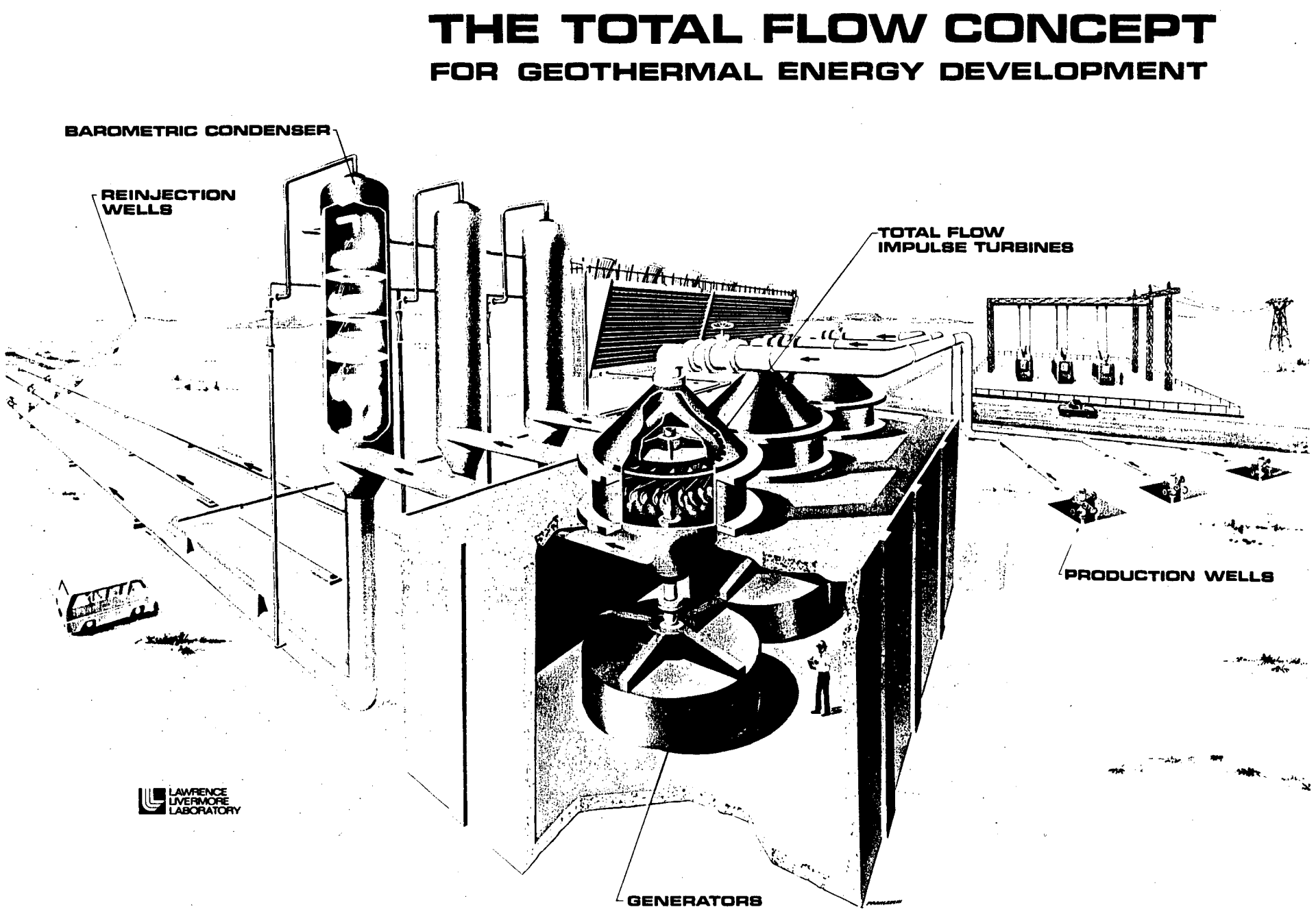

FIGURE 4-20. ARTIST'S CONCEPTION OF COMPLETE PLANT